THERMODYNAMIC PERFORMANCE ASSESSMENT OF A NEW THERMAL ENERGY STORAGE SYSTEM INTEGRATED WITHIN A SOLAR COMBINED POWER PLANT

2023
MASTER THESIS
MECHANICAL ENGINEERING

Aya Ahmed Faraj FARAJ

Thesis Advisor
Assist. Prof. Dr. Abdulrazzak Ahmed Saleh AKROOT

THERMODYNAMIC PERFORMANCE ASSESSMENT OF A NEW THERMAL ENERGY STORAGE SYSTEM INTEGRATED WITHIN A SOLAR COMBINED POWER PLANT

Aya Ahmed Faraj FARAJ

Thesis Advisor

Assist. Prof. Dr. Abdulrazzak Ahmed Saleh AKROOT

T.C.

Karabük University

Institute of Graduate Programs

Department of Mechanical Engineering

Prepared as a

Master Thesis

KARABÜK

June 2023

I certify that in my opinion the thesis submitted by Aya Ahmed Faraj FARAJ titled "THERMODYNAMIC PERFORMANCE ASSESSMENT OF A NEW THERMAL ENERGY STORAGE SYSTEM INTEGRATED WITHIN A SOLAR COMBINED POWER PLANT" is fully adequate in scope and in quality as a thesis for the degree of Master of Science.

Assist. Prof. Dr. Abdulrazzak Ahmed Saleh AKROOT .....
Thesis Advisor, Department of Mechanical Engineering

This thesis is accepted by the examining committee in a unanimous vote at the Department of Mechanical Engineering as a Master of Science thesis. June 20, 2023

Examining Committee Members (Institutions)	Signature
Chairman : Prof. Dr. Emrah DENİZ (KBU)	.....
Member : Assoc. Prof. Dr. Ali Etem GÜREL (DÜU)	.....
Member : Assist. Prof. Dr. Abdulrazzak AKROOT (KBU)	.....

The degree of Master of Science by the thesis submitted is approved by the Administrative Board of the Institute of Graduate Programs, Karabük University.

Prof. Dr. Müslüm KUZU .....
Director of the Institute of Graduate Programs

"I declare that all the information contained in this thesis has been gathered and presented in accordance with academic regulations and ethical principles, and I have, according to the requirements of these regulations and principles, cited all those which do not originate in this work."

Aya Ahmed Faraj FARAJ

ABSTRACT

M. Sc. Thesis

THERMODYNAMIC PERFORMANCE ASSESSMENT OF A NEW THERMAL ENERGY STORAGE SYSTEM INTEGRATED WITHIN A SOLAR COMBINED POWER PLANT

Aya Ahmed Faraj FARAJ

Karabük University
Institute of Graduate Programs
Department of Mechanical Engineering

Thesis Advisor:
Assist. Prof. Dr. Abdulrazzak AKROOT
June 2023, 51 pages

Renewable energies represent new options for sustainable electricity generation, necessitated by a sharp rise in energy demand, the limited availability of fossil fuels, and their damaging effects on the environment. One of the most promising technologies in electricity generation is that of concentrating solar power (CSP), which has the potential to provide an affordable solution to this problem. In this study, the findings of simulations and optimizations performed on solar-based triple combined cycles integrated with rock bed energy storage to produce electricity are presented to solve the issue of increasing demands for electricity in Iraq. Due to the sun's sporadic output, a thermal energy storage system using rock beds is built. Since the Rankin cycle can run independently thanks to rock bed storage, power may be generated at night or when solar energy is unavailable. The rock bed charges for 10 hours and discharges to run the Rankine cycle for 14 hours. The system's overall energy and

exergy efficiency was 38.95% and 42.84%, respectively. The total power produced in the system is 13,515 kW. The total power produced by the Rankine cycle is 4,089 kW, and the average system's electricity cost rate is 32.67 $/h.

The system was examined from the perspectives of a 3E approach (energy, exergy, and economics) and sustainability. A parametric analysis was carried out to examine the impact of different factors on system performance.

Key Words : Exergy economic, Solar energy, Exergy, Rock bed storage system**.**
Science Code : 91408

ÖZET

Yüksek Lisans Tezi

KOMBİNE GÜNEŞ ENERJİSİ SANTRALİNE ENTEGRE EDİLMİŞ YENİ BİR TERMAL ENERJİ DEPOLAMA SİSTEMİNİN TERMODİNAMİK PERFORMANS DEĞERLENDİRMESİ

Aya Ahmed Faraj FARAJ

Karabük Üniversitesi
Lisansüstü Eğitim Enstitüsü
Makine Mühendisliği Anabilim Dalı

Tez Danışmanı:
Dr. Öğr. Üyesi Abdulrazzak AKROOT
June 2023, 51 sayfa

Yenilenebilir enerjiler, enerji talebindeki keskin artışın, fosil yakıtların sınırlı mevcudiyetinin ve bunların çevre üzerindeki zararlı etkilerinin gerektirdiği sürdürülebilir elektrik üretimi için yeni seçenekleri temsil etmektedir. Elektrik üretiminde en umut verici teknolojilerden biri, bu soruna uygun fiyatlı bir çözüm sağlama potansiyeline sahip olan yoğunlaştırılmış güneş enerjisidir (CSP). Bu çalışmada, Irak'ta artan elektrik talebi sorununu çözmek için elektrik üretmek için kaya yatağı enerji depolaması ile entegre güneş tabanlı üçlü kombine çevrim üzerinde gerçekleştirilen simülasyon ve optimizasyonların bulguları sunulmaktadır. Güneşin düzensiz çıkışı nedeniyle, kaya yatakları kullanılarak bir termal enerji depolama sistemi inşa edilmiştir. Rankin döngüsü, kaya yatağı depolaması sayesinde bağımsız olarak çalışabildiğinden, geceleri veya güneş enerjisinin bulunmadığı zamanlarda güç üretilebilir. Kaya yatağı 10 saat şarj olur ve Rankine döngüsünü 14 saat çalıştırmak

için boşalır. Sistemin genel enerji ve ekserji verimliliği sırasıyla %38,95 ve %42,84 olmuştur. Sistemde üretilen toplam güç 13515 kW'dır. Rankine çevrimi tarafından üretilen toplam güç 4089 kW ve sistemin ortalama elektrik maliyet oranı 32,67 $/h'tir. Sistem, 3E yaklaşımı (enerji, ekserji ve ekonomi) ve sürdürülebilirlik açısından incelenmiştir. Farklı faktörlerin sistem performansı üzerindeki etkisini incelemek için bir parametrik analiz gerçekleştirilir.

Anahtar Kelimeler: Eksergoekonomik, Güneş enerjisi, Ekserji, Kaya yatağı depolama sistemi

Bilim Kodu **:** 91408

ACKNOWLEDGMENTS

I am deeply grateful to my advisor Assist. Prof. Dr. Abdulrazzak Ahmed Saleh AKROOT, for his unwavering support and guidance throughout my master's program. His expertise and patience have been invaluable to me and have played a crucial role in the success of this thesis.

I am grateful to the University of Karabük for providing me with the opportunity to conduct my research, and for all the resources and support they provided.

Thanks go to my friends and family for their love and support during this process. Without their encouragement and motivation, I would not have been able to complete this journey.

I would like to extend my sincere gratitude to all the participants in my study. Their willingness to share their experiences and insights has been invaluable to my research and has helped to make this thesis a success. Thank you for your time and contribution. Finally, I am grateful to everyone who has supported me throughout this process. Without your help and guidance, this thesis would not have been possible.

CONTENTS

Page

Page

LIST OF FIGURES

Page

LIST OF TABLES

Page

SYMBOLS AND ABBREVIATIONS

SYMBOLS

P	: Pressure
T	: Temperature
h_c	: Convective heat transfer coefficient of air
T_{out}	: Outlet temperature
PR	: Pressure ratio of the compressor
η_c	: Isentropic efficiency of the compressor
K	: Specific heat rate of the air
$\dot{m}$	: Mass flow rate of the air
η_{gen}	: Generator efficiency
$\dot{m}_g$	: Flow rate of the combustion gases (kg/s)
T_m	: Mean temperature (℃)
T_0	: Ambient temperature (℃)

ABBREVIATIONS

BC	: Brayton cycle
RC	: Rankine cycle
ORC	: Organic Rankine cycle
GT	: Gas turbine
CC	: Combustion chamber
AC	: Air compressor
P	: Pump
Con	: Condenser
ST	: Steam turbine
HRSG	: Heat recovery steam generation
HE	: Heat exchanger

ORT : Organic Rankine turbine

HRB : Heat recovery boiler

GTIT : Gas turbine inlet temperature

EES : Engineering equation solver

TES : Thermal energy storage

CFD : Computational fluid dynamics

HTTES : High-temperature thermal energy storage

LCOE : Levelized cost of electricity

LCOW : Levelized cost of water

PTS : Power tower systems

LTNE : Local thermal non-equilibrium

LTE : Local thermal equilibrium

$STESM_S$: Sustainable thermal energy storage materials

STES : Sensible thermal energy storage

PCM_S : Phase change materials

ORS : Organic Rankine cycle

GTC : Gas turbine cycle

RBES : Rock bed thermal energy storage

SPECO : Specific exergy costing

HTF : Heat transfer fluids

PART 1

INTRODUCTION

1.1. OVERVIEW

A solar thermal power plant incorporating thermal energy storage (TES) represents one of the available renewable energy sources [1]. In contrast to power plants that are reliant on fossil fuel resources and emit harmful substances, solar thermal power plants harness the copious and readily accessible energy of the sun. Through the conversion of solar heat into electricity, these power plants make a significant contribution towards mitigating greenhouse gas emissions and addressing the issue of climate change [2,3].

Utilizing a solar thermal power plant that integrates thermal energy storage is a novel approach that effectively captures solar energy to produce electrical power while integrating a storage mechanism that ensures a consistent power supply, even during periods of limited sunlight. A solar thermal power plant employs solar collectors to capture and transform solar radiation into thermal energy. It is subsequently used to produce electricity using a variety of approaches, such as thermoelectric generators, gas turbines or steam turbines [3, 4].

The thermal energy storage system is a crucial element of a solar thermal power plant as it enables the facility to accumulate surplus thermal energy during periods of ample sunlight and subsequently utilize it during periods of limited sunshine or absence of sunlight. The augmentation of storage capacity fortifies the dependability of the plant. It empowers it to generate electrical power without interruption, even without sunlight due to nighttime or overcast weather conditions [5, 6].

Integrating solar collectors [8] and thermal energy storage in a solar thermal power plant yields various benefits. Initially, it provides a sustainable and environmentally friendly energy source through solar radiation [9]. Reducing greenhouse gas emissions and decreasing reliance on fossil fuels are significant factors in promoting a sustainable energy blend. Implementing a thermal energy storage system improves the plant's dispatchability, enabling it to deliver a reliable and uniform power output, even in the face of variable solar radiation. This characteristic is important in fulfilling electricity requirements during high-demand periods or when clouds intermittently obstruct sunlight. Finally, the extended longevity and minimal upkeep demands of solar thermal power facilities renders them appealing prospects for sustained energy production [10].

Solar thermal power plants that incorporate thermal energy storage exhibit potential as a viable option for sustainable and dependable electricity production. These power plants harness the plentiful and environmentally friendly energy from the sun while also integrating energy storage technology to guarantee an uninterrupted power supply [11].

1.2. THERMAL ENERGY STORAGE

Thermal energy storage (TES) systems are an exciting technology with the potential to play an essential part in the future of energy. TES systems can aid in decreasing our reliance on fossil fuels, enhancing the efficacy of our energy systems, and minimizing our environmental impact [12]. TES refers to storing energy in the form of heat or cold by heating or cooling a medium, which can be utilized later as required. Using thermal energy storage may also help to equalize daytime and nighttime power demands [13,14]. TES has several potential uses, including but not limited to the following [15]:

- Water heating.
- Space heating and cooling.
- Power generation.
- Industrial processes.

1.3. BENEFITS OF USING THERMAL ENERGY STORAGE

The utilization of thermal energy storage in various fields has long been established [8, 9] not only in residential applications but also in district heating, as mentioned in [10] and in commercial and industrial applications, as mentioned in [11]. The main advantages deriving from the application of a thermal storage system can be summarized as follows [12-14]:

- Reduced energy costs: TES systems reduce total energy costs by storing energy during off-peak hours and releasing it during peak hours. Any peak demand costs may be avoided, and grid stability may improve in this way.
- Increased reliability: By functioning as a backup power source in an outage, TES systems contribute to the overall dependability of the energy grid. This may lessen the effect of power outages on companies and consumers by keeping essential loads operating during blackouts.
- Improved efficiency: By storing energy during periods of high efficiency and discharging it during periods of low efficiency, TES systems can increase the efficiency of energy systems. This can help reduce a system's total energy consumption.
- Environmental benefits: By lowering the demand for power during peak hours, TES systems may help to lessen negative environmental effects. This could reduce the amount of harmful gases released into the atmosphere.
- Increased productivity: Energy may be stored in TES systems for use in industrial activities, which may assist to increase production while decreasing expenditures.
- Improved comfort: Using TES systems to store heat or cold may enhance building occupant comfort. This may assist in cutting down on the amount of money and energy spent on cooling and heating homes.
- Reduced emissions: TES may aid in minimizing emissions. For instance, TES may be utilized for storing heat from solar energy systems, which may decrease reliance on fossil fuels [19] for power generation.

1.4. DISADVANTAGES OF USING THERMAL ENERGY STORAGE

The following is a summary of the disadvantages associated with thermal energy storage (TES) [20–22]:

- Limited storage capacity: TES systems can only store a certain quantity of energy due to their limited capacity. The storage capacity that TES systems can store varies according to the size of the system, the kind of TES system, and the operating conditions.
- High cost: The installation and operation of TES systems can incur significant costs. The pricing of TES systems is based on the system's specific type, magnitude, and geographical placement.
- Low efficiency: Thermal Energy Storage (TES) systems may exhibit inefficiencies, resulting in the dissipation of a portion of the stored energy during storage and retrieval operations. The efficiency of TES systems relies on the kind, size, and operating conditions of the system.
- Technical challenges: The design, installation, and operation of TES systems can present a complex undertaking. The complexity of TES systems varies based on the nature and size of the system.

1.5. ROCK BED ENERGY STORAGE

Rock bed energy storage (RBES) is a kind of thermal energy storage (TES) that uses a bed of rocks to store heat. The rocks are often heated by a heat pump or a solar thermal collector, and the heat may then be released to warm or cool the surrounding environment [23]. Most RBES systems are large and have a large heat storage capacity [24]. They are thus ideal for applications where a large quantity of heat has to be stored, such as power-generating systems. Additionally, RBES systems are a reliable and cost-effective way to store heat. The typical heat loss from an RBES system is less than 13% [25]. This makes them suitable for applications that prioritize efficiency, such as industrial processes. RBES systems have advantages, such as large storage capacity, high efficiency, and mature technology. Nevertheless, the initial cost of RBES systems is high and requires a large size.

1.6. AIM OF THE STUDY

The present thesis proposes and examines a triple-cycle power plant that utilizes solar energy as its primary source. The proposed power plant is integrated with rock bed energy storage to ensure a consistent power supply, even during periods of limited sunlight. A comprehensive analysis of the energy, exergy, and economics of rock bed storage has been conducted. No prior development or exergetic study of a thermal energy storage system utilizing a rock bed has been documented in the available literature. The exergy efficiencies, exergy destruction, initial cost investment, and cost of exergy destruction of all components in a triple-cycle power plant have been computed and juxtaposed to provide a more comprehensive understanding of their respective functions. Additionally, parametric analyses are carried out to assess the impact of fluctuating state properties and operational parameters on the work net, overall efficiencies, and specific costs of the triple-cycle power plant. Therefore, the novelty of this work lies in the investigation of the performance of a solar-based triple combined cycle with a rock bed thermal storage unit and the analysis of the effects of varying parameters on the system's efficiencies and cost. The achieved objectives of thermodynamic and exergo-economic analysis of the triple-cycle power plant are summarized as follows:

- A novel triple-cycle power plant based on solar energy as a primary source has been proposed and investigated.
- The technology for storing heat in rock beds has been improved and refined.
- Energy, exergy, and economic analyses of the proposed system have been conducted comprehensively.
- The exergy efficiencies, exergy destruction, initial cost investment, and cost of exergy destruction of all components have been computed and compared to provide a clearer picture of their respective functions within a triple-cycle power plant.
- The impacts of different parametric studies and operating conditions on the performance of the proposed system have been analyzed.

Overall, the objectives of thermodynamic and exergo-economic analysis are to improve the proposed system's efficiency, reliability, and cost-effectiveness and contribute to developing a more sustainable and reliable energy future.

1.7. OUTLINE OF THE THESIS

Chapter 1 presents an introduction to the present work, general information on thermal energy storage, the advantages and disadvantages of thermal energy storage, and the main objectives of the current work. Chapter 2 illustrates the literature related to this study. Chapter 3 explains the main components and operation work of the proposed model for this thesis. This chapter also contains the input parameters to the system and the thermodynamic and exergo-economic equations used in the system's energy, exergy, and economic analysis. Chapter 4 contains the findings and discussion. Finally, Chapter 5 includes the conclusion and presents possible future efforts.

PART 2

LITERATURE REVIEW

Many studies have been focusing on thermal energy storage systems and the integration of these systems with power plants. Muhammed et al. [26] examined the utilization of rock-based thermal energy storage systems in industrial applications, specifically focusing on their integration with solar thermal collectors. The study encompassed a range of subjects, including the modelling and optimization of system design, experimental validation, and a parametric analysis. The use of computational fluid dynamics (CFD) in modelling these systems and recent developments in the field are also discussed. The findings indicated that in the process of simulating TES systems that rely on rock-based materials, it is crucial to consider the influence of repeated charge-discharge cycles, as well as the ramifications of each heat transfer mechanism during each operational phase. The thermal energy storage system's energy storage capacity and energy loss through the outlet and walls can be influenced by the particle size of the rock.

Knobloch et al. [25] examined a range of studies on using rocks as a medium for TES in a pilot plant. The authors assessed the possible deterioration of the RBTES system, examining both the material and system-level factors. Their findings include insights into modifications at the system level and techniques for characterizing materials at the microscale. The study has indicated that rocks that contain anhydrous minerals and exhibit a high heat capacity are optimal for thermal energy storage (TES) systems. Furthermore, it has been observed that the specific heat capacity of rocks undergoes changes during the initial heating cycles but eventually stabilizes at an equilibrium state.

Soprani et al. [27] researched a prototype rock bed for TES at high temperatures. The investigation focused on the influence of buoyant forces on the temperature gradient

inside the bed and the efficacy of the storage unit. To maximize storage operations, rock bed configurations, flow concepts, and various charging powers were debated, resulting in a 17% increase in the efficiency of the charging phase. In addition to discussing the use of rock beds as a TES system for CSP, the results included design considerations and correlations for RBTES in power plants. The authors also noted that the heat losses in the inlet pipelines and at the outflow have a major influence on the thermal efficiency of the storage and that thermal integration of the storage facility should receive special attention.

Marongiu et al. [28] presented a 2D numerical model for high-temperature thermal energy storage (HTTES) using a rock bed that was validated against experimental data. The effects of many factors on the efficiency of the storage system were analyzed, such as the insulating material, air flow rate, rock size, and rock type. The results indicated that decreasing rock size contributed primarily to supplying a steeper temperature gradient in the rock bed, decreasing discharge losses, and increasing charge efficiency. In addition, the study emphasized the significance of insulation in HTTES, particularly in small-scale systems. Overall, the study offers guidelines for the industrial design and operation of HTTES units.

Nahhas et al. [29] examined the utilization of basalt rocks as a storage medium for high-temperature CSPs. The research assessed the mineralogical composition, structural examination, mechanical characteristics, and thermal response of two distinct types of basaltic rocks obtained from disparate locations. The findings indicate that basalt rocks possess favorable characteristics for employment in (TES) systems, such as elevated density, thermal capacity, and thermal conductivity. The authors put forth the proposition that basalt rocks may serve as a viable substitute for other thermal energy storage (TES) materials. Furthermore, they presented empirical evidence that can be utilized for computational simulations aimed at devising storage systems and forecasting their efficacy.

Desai et al. [30] performed a technical evaluation of various thermal energy storage technologies for a medium-scale cogeneration plant, utilizing a unique micro-structured polymer foil-based CSP. The research conducted a comparative analysis of

two-tank direct storage, two-tank indirect storage, and RBTES while considering various heat transfer fluids and rock types. The findings indicated that utilizing packed-bed rock thermocline storage with Therminol 55 as the HTF and quartzite rock is the optimal choice. This approach yields a reduced levelized cost of electricity and fresh water compared to the conventional two-tank indirect storage method. The study additionally deliberated on the conceptualization and enhancement of CSP facilities featuring diverse TES arrangements, appraising the levelized cost of electricity (LCOE) and the levelized cost of water (LCOW) for the system. The document references a range of scholarly sources, including studies and reports that explore diverse facets of renewable energy technologies. These include solar power plants, desalination solutions, organic Rankine cycle systems, hydrogen production, and heat transfer fluids.

Zanganeh et al. [31] proposed using a packed bed of rocks and air as a thermal energy storage system for CSP plants. A TES unit at a pilot scale was designed and subjected to testing. Additionally, a dynamic numerical model for heat transfer was formulated and verified. The model was designed to optimize and scale up the design of a TES system at an industrial scale for a CSP plant, and contained changing thermo-physical parameters for both fluid and solid phases. The use of rock beds and air provided a number of benefits, such as low cost, a large usable temperature range, direct heat transfer between the working fluid and the storage material, and the absence of any potential safety hazards.

Heller and Gauche [32] investigated the modelling, design, and optimization of a TES system using a packed bed of rocks for a combined cycle solar thermal power plant in South Africa. The article includes a 1D model based on the E-NTU approach, which is validated using experimental data from previous studies. Sensitivity analyses were conducted to calculate the effect of changes in several variables on the levelized cost of electricity (LCOE). The results showed that plant control has the most significant impact on costs, and the LCOE is slightly higher than some other CSP designs. The article also cited various studies on mass transfer, thermal performance, pressure drop, Nusselt number, friction factor correlations, thermal conductivity, and costs for PTC and power tower systems in the US market.

Beaujardiere et al. [33] discussed using numerical models to simulate the performance of gas-solid PB-TES systems in concentrated solar power plants. The research compared and assesses the computational efficiency and fidelity of local thermal non-equilibrium (LTNE) and local thermal equilibrium (LTE) models. The authors also discussed the challenges of numerical instability and the importance of grid independence in numerical simulations. The research findings indicate that the utilization of the LTE model can result in a significant reduction in computational expenses. However, it is important to note that this approach may lead to an underestimation of the blowing work due to the mean equivalent fluid temperature in the bed being underestimated. The authors proposed the utilization of spatial discretization with high resolution and temporal discretization with low resolution for the Effectiveness-NTU-LTNE model. The study's findings offer valuable insights into the utilization of local thermal equilibrium (LTE) and local thermal non-equilibrium (LTNE) assumptions in the performance modelling of CSP-packed bed TES systems. Kocak and Paksoy [34] described a study on using demolition waste as a sustainable and low-cost material for TES in a lab-scale packed bed system. The experimental setup involved subjecting the system to varying operational parameters, followed by a comparative analysis with respect to the performance of Therminol 66 synthetic oil as a liquid medium for heat storage. According to the research, the utilization of demolition waste STESMs as a fluid storage material outperforms the utilization of Therminol 66 synthetic oil. Additionally, the system's net storage capacity is observed to increase with an increase in the inlet HTF temperature. The findings showed that the utilization of packed-bed thermal energy storage (TES) system containing sustainable thermal energy storage materials (STESMs) derived from demolition waste exhibits superior performance compared to the utilization of Therminol 66 synthetic oil as a liquid storage medium.

Abdulla and Reddy [35] investigated the thermal performance of a molten salt packed-bed thermocline TES system for CSP plants. The investigation utilized numerical simulations to analyze the impact of diverse operational parameters on the efficacy of the system. The study offered a valuable understanding of the pertinent parameters that necessitate consideration during the design phase and the optimal operating procedures to guarantee efficient performance. The study has revealed that the primary factor that

determines the efficiency of the system is the range of operating temperature. Additionally, it has been observed that the efficiency of discharging tends to decline as the operating temperature difference increases. The study determined that the efficiency of the system was primarily influenced by two key design and operating parameters, namely the effective diameter of the filler and the range of operating temperatures.

Öztürk et al. [36] presented a thermodynamic model of a solar energy-based combined cycle with an RBTES system. Parametric studies were conducted to determine the effects of different state properties and operating conditions on the system's energy and exergy efficiencies. The study also investigated the impact of changing variables such as inlet temperature and air mass flow rate on the system's performance. The research findings indicate that the performance of the system is notably influenced by the air inlet temperature and mass flow rate. Additionally, the rock bed energy storage mechanism is charged through the utilization of hot exhaust gas coming from the gas turbine. According to the results, the overall combined system's energy and exergy efficiencies are 69.2% and 37.3%, respectively.

Sharma et al. [37] discussed the optimization of PB-TES systems for CSP plants. The study used a thermo-economic model to assess system performance under various operating circumstances and input parameters. The study explained the approach for designing and analyzing the PB-TES system. The findings indicate that adopting the PB-TES technology can improve the operational efficiency and financial feasibility of CSP plants. The study also conducted an analysis of three discrete types of sensible thermal energy storage (STES) mediums in order to enhance the performance of the PB-TES system in a combined CSP and CO_2 Rankine facility.

Fernández et al. [38] discussed the use of PB-TES systems as a promising alternative for thermal efficiency and economic viability. The authors proposed operation strategies and thermal management guidelines for such systems, using low-cost by-product materials such as steel slag as a heat storage medium in the packed bed. The research examined three distinct thermal exploitation scenarios and determined that appropriate optimization of the PB-TES system, coupled with effective thermal management, can result in significant thermal efficiency gains.

Abdulla and Reddy [39] performed a study that compares single and multi-layered PB-TES systems for concentrated solar power plants. According to the findings, the multi-layered system with phase change materials (PCMs) provided an extra hour of discharge in comparison to the utilization of a single-layered system. The authors also discussed the numerical modelling and analysis of a multi-layered PB-TES system for CSP plants, including the effect of the intermediate melting temperature range of PCMs. The study concludes that the multi-layered system offers the most promising opportunities for achieving a smooth integration into CSP facilities, while also attaining the desired level of efficiency. The study also indicated that disregarding radial temperature change is a valid approximation, and the tank's axial temperature variation helps to explain heat transmission.

Saha and Dus [40] examined the energetic and exergetic performance of PBTESs filled with encapsulated phase change materials (PCMs). The study covered various aspects of PBTESs, including numerical modeling, heat transfer characteristics, efficiency, and optimization. The study investigated the impact of different parameters, including capsule diameter, mass flow rate, and bed height, on the efficiency of PBTESs. The results showed the importance of exergy analysis in optimizing the performance of PBTESs for solar thermal applications. The utilization of spherical capsules that have different diameters and contain PCM has the capability to enhance the PB-TES systems. The exergy efficiency of spherical capsules that encase ice within a storage tank is greater when the HTF inlet temperature is closer to the solidification temperature of the water. The optimization of the performance of the PBTES thermal can be achieved by varying parameters such as mass flow rate, capsule diameter, and bed height.

Amiri et al. [41] presented a comprehensive review of RBTES systems used for storing and releasing heat energy. The study covered the technical and non-technical aspects of RBTES systems, including their design criteria, materials used for storage, applications, and potential for energy conservation and reducing carbon emissions. The study also provides a list of references related to TES systems and discusses various studies and experiments related to PB-TES systems and HTTES in CSP plants. According to the study, RBTES has significant potential as a sustainable energy

storage solution, but further research and development are needed to optimize its performance and cost-effectiveness.

Rahbari et al. [42] discussed the design, performance, and feasibility of a hybrid energy storage system that combines HTTES with an organic Rankine cycle (ORC) to achieve higher electrical efficiency. The study investigated thermodynamic performance, environmental effectiveness, cost-effectiveness, and the effects of partial load operation on the system's techno-economic indices. The off-design operation analysis and system performance optimization have been included. The findings revealed that the hybrid system is highly energy efficient and economically feasible, with the potential to reduce greenhouse gas emissions. The system can reduce CO_2 emissions by 33,731 tons and NOx emissions by 25,000 tons annually. The system's operational conditions significantly impact its performance, and it is imperative to maintain the system's operation in proximity to its nominal design conditions.

Zhang et al. [43]investigated the feasibility of incorporating HTTES into thermal power plants to improve their flexibility and peak shaving capabilities. The study explored the effect of thermal energy temperature, pipeline pressure loss, and regulating valve opening on the thermal efficiency of the plant. The study concluded that HTTES can enhance the utilization of wind power and potentially address the challenge of scaling up renewable energy consumption. The findings indicate that the incorporation of HTTES technology in thermal power plants is a viable option that can enhance the utilization of wind power and concurrently decrease the coal combustion rate of the power generation process. The incorporation of HTTES technology in thermal power plants has the potential to enhance the dynamic performance of these plants, enable flexible operation, minimize peak-to-valley gaps, and optimize the rated load operation time cycle.

Codd et al. [44] discussed various technologies and materials used in TES systems for CSP plants, as well as recent advances in CSP receiver and TES technologies. The study also covered the properties, performance, and challenges of different types of heat transfer fluids (HTF) and thermal storage media used in CSP systems.

Geu et al. [45] investigated a thermodynamic model for a PB-TES system with fixed temperatures on both ends. The model calculated key parameters such as thermocline thickness, exergy destruction, thermal storage time, and thermal storage capacity. The study also investigated the stable operation of the PBTES device, pinpointing aspects that might reduce exergy destruction and lead to a higher stable operation cycle count. The findings indicate that a decrease in temperature difference and an increase in the inlet temperature of hot air led to reduced exergy destruction and increased cycle numbers of stable operation. The increase in thickness of the thermocline results in a reduction of the thermal storage capacity of the PBTES.

Bhardwaj et al. [46] discussed the use of RBTES systems for solar energy applications. This study covered various mathematical models used to predict the behavior of RBTES systems, recent studies and experiments conducted on these models, and the advantages of using rock bed systems, including their simplicity, low cost, and low-pressure drop. The study also examined the thermal models utilized in packed beds and the underlying assumptions commonly employed for mathematical evaluations of heat transfer in RBTES. The results conclude that RBTESs have several advantages, including simplicity, low cost, and low-pressure drop.

Kunwer and Pandey [47] discussed the analysis and optimization of a PB-TES thermocline tank for concentrated solar power applications. The study investigated the effect of parameters such as void fraction, pebble diameter, and mass flow rate on charging efficiency and pressure drop. They determined the optimal parameters that result in minimum pressure drop and maximum efficiency in thermocline systems and subsequently examined the limitations and challenges associated with using these systems in industrial settings.

The present study examines the impact of pebble diameter on the efficiency of charging and pressure drop. The results indicate that the optimal pebble diameter for achieving maximum efficiency and minimal pressure drop is 0.03. The research findings indicated that the efficacy of the TES mechanism is significantly influenced by the efficiency of its charging and discharging processes, as well as the magnitude of the pressure drop being experienced.

Eddemani et al. [48] developed and evaluated the performance of an air-rock bed solar energy storage system during the discharge process. The study investigated the effect of the number of thermal cycles and the outlet temperature of the mass flow rate on the air, the thermal behavior of the rock bed, and the amount of energy recuperated during the discharge process. The findings would facilitate comprehension of the thermal behavior and enable assessment of the performance of the storage mechanism during the discharge stage. This aspect has yet to be subjected to rigorous scrutiny akin to the charging phase. The investigation introduced a quantitative framework for a thermal energy storage mechanism that employs rocks as the storage medium and air as the heat transfer agent. The findings presented that increasing the mass flow rate decreases the time of the discharge process and increases thermal performance. The energy recovery rate would experience an upward trend as the cycle number increases until it eventually reaches a state of cyclic equilibrium.

PART 3

SOLUTION METHODOLOGY

The triple-cycle power plant consists of a Brayton cycle as the primary cycle and a Rankine cycle and an organic Rankine cycle as the secondary cycles. This study selected the province of Salahaddin in Iraq to get the data. In Figure 3.1, the schematic view of the triple-cycle power plant designed within the scope of this thesis is given. Solar energy and fuel energy are used in the system. There are heliostats, solar receivers, gas turbine cycle (GTC), rock bed thermal energy storage (RBES), Rankine cycle (RC), and organic Rankine cycle (ORC) in this system.

The air compressor compresses the ambient air to up to 1.62 MPa pressure, and then it is heated by a central receiver. Therefore, a combustion chamber makes up for any lack of solar light to keep the gas turbine's inlet temperature steady during charging. As a result, enough thermal energy will be stored in the rock bed storage tank to allow the system to produce power at night when there is no solar radiation. Nevertheless, high efficiency for the system will be enhanced if the air temperature at the gas turbine inlet reaches up to 1,000℃.

The Rankine steam cycle is powered by the hot exhaust gas from the gas turbine, which is stored in a rock bed thermal energy storage tank. In addition, the organic Rankine cycle is powered by the hot air that is evacuated from the rock bed storage tank.

The Brayton cycle runs for 10 hours, during which time solar radiation is most effective, after which the Rankine cycle would be discharged during the remaining 14 hours of the day.

The thermodynamic and thermo-economic assessments are based on the following presumptions:

- The pressure (P_o) and the temperature (T_o) at the reference state are 1 bar and 25℃, respectively.

- The energies, both kinetic and potential, are fixed.
- The system's steady-state operating conditions are considered. There is an assumption of stable operating conditions for all cycles in the system during their operation periods due to the projected constancy of solar radiation throughout the day.
- Working fluids for the Brayton, Rankine, and organic Rankine cycles are air, water, and R600a, respectively.
- The compressor, pump, and turbines operate in an adiabatic process.
- The sun's temperature is estimated to be 6,000 K.

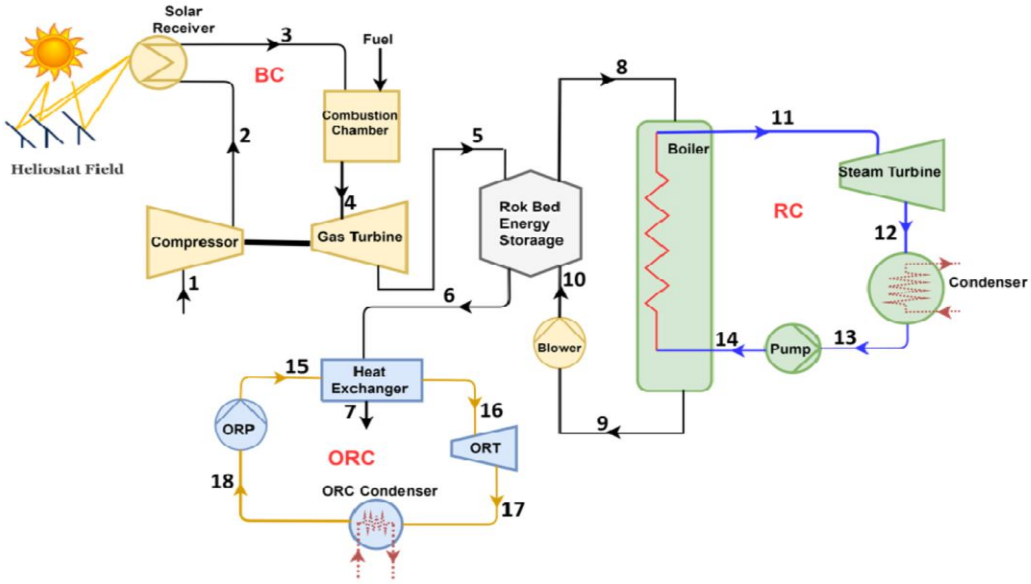

Figure 3.1. Schematic diagram of the triple cycle power plant.

Each component in the triple-cycle power plant is separately thermodynamically modelled. In the system, equations were created for mass, energy, exergy, and energy-economic analyses. Table 1 lists the operational and technical parameters used in the analysis.

Table 3.1. Operation conditions used for the triple-cycle power plant.

Component	Parameter	Value
Compressor	Compression ratio	16.2
	Inlet temperature	25℃
	Inlet pressure	100 kPa
	Isentropic efficiency	84%
	Air flow rate	51.67 m^3
Heliostats field	Area	53935 m^2
Gas turbine	Pressure ratio	15.2
	Inlet temperature	1000℃
	Isentropic efficiency	85%
Steam turbine	Inlet pressure	5000 kPa
	Isentropic efficiency	80%
Condenser	Condenser temperature	60℃
Pump	Isentropic efficiency	90%
Organic Rankine cycle turbine	Inlet pressure	1700 kPa
	Isentropic efficiency	85
Organic Rankine cycle condenser	Condenser pressure	635.7 kPa
Organic Rankine cycle pump	Isentropic efficiency	90%

3.1. THERMODYNAMIC ANALYSIS

The mass, energy, and exergy equations of the system are written separately for the general system and for each component.

The mass balance equation of the system is written as:

$$\sum \dot{m}_{in} = \sum \dot{m}_{out} \quad 3.1$$

The overall energy balance of the system is shown by the following equation [49,50]:

$$\dot{Q}_{in} + \dot{W}_{in} + \sum \dot{m}_{in} h_{\text{in}} = \dot{Q}_{out} + \dot{W}_{out} + \sum \dot{m}_{out} h_{out} \quad 3.2$$

The general exergy balance of the system can be written as [51,52]:

$$\sum (\dot{m}ex)_{in} + \dot{E}x_{in,W} + \dot{E}x_{in,Q} = \sum (\dot{m}ex)_{out} + \dot{E}x_{\text{out},W} + \dot{E}x_{\text{out},Q} \quad 3.3$$

$$\dot{E}^{Q} = \dot{Q}\left(1 - \frac{T_0}{T_s}\right) \quad 3.4$$

$$\dot{m}_{\text{in}}\, S_{\text{in}} + \left(\frac{\dot{Q}}{T}\right) + \dot{S}_{\text{gen}} = \dot{m}_{\text{out}}\, S_{\text{out}} \tag{3.5}$$

he heat transfer rate between the solar receiver and the air can be estimated as follows [51,53]:

$$\dot{Q}_{\text{Solar}} = \dot{Q}_h - \dot{Q}_{\text{rec,loss}} \tag{3.6}$$

$$\dot{Q}_{\text{Solar}} = \dot{m}_3 h_3 - \dot{m}_2 h_2 = \dot{m}_3 c_{p,3} T_3 - \dot{m}_2 c_{p,2} T_2 \tag{3.7}$$

The following formulas can be used to determine the heat transfer rate measured in the heliostat field and the receiver heat loss rate [54]:

$$\dot{Q}_h = A_h \times N \times I \times \eta_h \tag{3.8}$$

$$\dot{Q}_{\text{rec,loss}} = \dot{Q}_{\text{conv}} + \dot{Q}_{rad} = A_r \times [h_c \times (T_r - T_0) + \sigma \times \varepsilon \times (T_r^4 - T_0^4)] \tag{3.9}$$

From the literature review, the convective heat transfer coefficient of air (h_c) in W/m^2K units can be calculated as follows [55]:

$$h_c = 10.45 - V + 10\sqrt{V} \tag{3.10}$$

The outlet temperature of the compressor used in the gas turbine cycle and the power required for the compressor are calculated from Equations below [56]:

$$T_{\text{out}} = T_{\text{in}} \left(1 + \frac{1}{\eta_{AC}} \left(P_{r,AC}^{\frac{k_{air}-1}{k_{air}}} - 1\right)\right) \tag{3.11}$$

$$\dot{W}_{AC} = \dot{m}_{air} * (h_{\text{out}} - h_{in}) \tag{3.12}$$

$P_{r,AC}$ and η_{AC} are the pressure ratio of the compressor and the isentropic efficiency of the compressor, respectively, and k_{air} and $\dot{m}_{air}$ are the specific heat rate of the air and the mass flow rate of the air (in kg/s), respectively. The gas turbine outlet temperature and the power produced in the turbine are found with the help of the following equations [57,58]:

$$T_{GT,\,\text{out}} = T_{GT,\,\text{in}} \left(1 - \eta_{GT}\left(1 - P_{r,GT}^{\frac{1-k_{air}}{k_{air}}}\right)\right) \quad 3.13$$

$$\dot{W}_{GT} = \dot{m}_{GT,in} * \left(h_{GT,\,\text{in}} - h_{GT,\,\text{out}}\right) \quad 3.14$$

$$\dot{W}_{GT,net} = \eta_{GEN} * \left(\dot{W}_{GT} - \dot{W}_{AC}\right) \quad 3.15$$

$P_{r,AC}, \eta_{AC}$, η_{GEN}, k_{air} and $\dot{m}_{GT,in}$ used in the equation respectively denote the turbine pressure ratio, isentropic efficiency of the turbine, generator efficiency, specific heat ratio for air and flow rate of the combustion gases (in kg/s).

The thermodynamic model created for the thermal energy storage tank calculations can be made by calculating the heat loss from the thermal energy storage tank in the system to the environment. First, the total heat loss coefficient from the storage to the ambient air (*U*) is calculated, then the total heat loss is calculated with the following equation [36,59]:

$$\dot{Q}_{\text{loss}} = U \times A \times (T_m - T_0) \quad 3.16$$

where A is the total surface area of the rock bed storage tank (in m^2), T_m the mean temperature (in °C), and T_0 the ambient temperature (in °C). There are three different operating modes in the thermal energy storage tank: charging, discharging and storage. The total amount of energy stored during the charging period is calculated using the following equations [36]:

$$Q_{\text{charging}} = (m_5 h_5 - m_6 h_6) \times 3600 \times t_{charging} \quad 3.17$$

$$Q_{\text{charging}} = m_{rock}\, c_{rock} (T_5 - T_0) \quad 3.18$$

where $t_{charging}$ is the charging time, c_{rock} the specific heat of the rock (c_{rock} =0.840 kJ/kg K), and m_{rock} the mass of the rock. The following equation is used for the total heat loss calculations during the storage period.

$$Q_{\text{charging}} = Q_{\text{discharging}} + Q_{\text{loss}} \quad 3.19$$

The heat transferred to the multi-generation system during the discharge period is calculated as follows [36]:

$$Q_{\text{discharging}} = (m_8 h_8 - m_{10} h_{10}) \times 3600 \times t_{\text{discharging}} \quad 3.20$$

$$Q_{\text{discharging}} = m_{\text{rock}}\, c_{\text{rock}}\, (T_5 - T_0) \quad 3.21$$

where $t_{\text{discharging}}$ is the discharging time. The energy and exergy equations for the components used in the system are shown in Table 3.2. Fuel and product exergy for each component are shown in Table 3.3.

The First and Second Law efficiencies of the triple combined cycle can be determined thus [60,61]:

$$\eta_{\text{I}} = \frac{\dot{W}_{\text{net}}}{\dot{Q}_{\text{in}}} \quad 3.22$$

$$\eta_{\text{II}} = \frac{\dot{W}_{\text{net}}}{\dot{E}x_{in}} \quad 3.22$$

The power output from the triple combined system can be found thus:

$$\dot{W}_{\text{net}} = \dot{W}_{\text{GT}} - \dot{W}_{\text{Comp}} + \dot{W}_{ST} - \dot{W}_{\text{Pump}} - \dot{W}_{\text{Blower}} + \dot{W}_{ORT} - \dot{W}_{\text{ORP}} \quad 3.23$$

The heat and exergy input of the system can be determined as follows:

$$\dot{Q}_{in} = \dot{Q}_{Fuel} + \dot{Q}_{\text{Solar}} \quad 3.24$$

$$\dot{E}x_{in} = \dot{E}x_{Q,Fuel} + \dot{E}x_{\text{Solar}} \quad 3.25$$

3.2. EXERGY ECONOMIC ANALYSIS OF THE SYSTEM

With the exergy-economy model, both exergy analyses, and cost analyses are made in thermodynamic systems, and the two models are combined. There are different thermos-economic analysis methods in the literature, and in this thesis study, the SPECO method was used. For the implementation of the SPECO (Specific Exergy Costing) method, the cost of each product is obtained by calculating the exergy current at each point and the costs for each current. The results are calculated by creating exergy-cost balance equations for each component [62–64].

The general exergy-cost balance equation for each component in the system can be written as follows [65]:

$$\sum \dot{C}_{in,k} + \dot{C}_{Qk} + \dot{Z}_k = \sum \dot{C}_{out,k} + \dot{C}_{w,k} \quad 3.26$$

where $\dot{C}_{Qk}$, and $\dot{C}_{w,k}$ are the heat and power exergy cost flow, respectively, and $\dot{Z}_k$ the capital cost, operation and maintenance cost flow, which is calculated according to the formula below [66]:

$$\dot{Z}_k = Z_k^{CI} * CRF * \frac{\phi}{t} \quad 3.27$$

The variables Z_k^{CI}, CRF, ϕ and t in the equation are the investment cost of the components, the return on capital factor, and the maintenance factor and the annual

operating time of the system, respectively. In this study, the total annual working time is taken as 8,640 hours. The CRF value is calculated with the following formula [67]:

$$CRF = \frac{i(1+i)^N}{(1-i)^N - 1} \tag{3.28}$$

The interest rate *i* is accepted as 12%, and *N* is the total system life of 20 years [68]. The exergy cost flow for each point in the system is calculated with the following formula:

$$\dot{C} = c\dot{E}x \tag{3.29}$$

$\dot{E}x$ denotes exergy current and *c* denotes the specific exergy cost. One of the important parameters used to determine the performance of the system is the exergy-economic factor, denoted by f_k, which is calculated with the equation below [69,70].

$$f_k = \frac{\dot{Z}_k}{\dot{Z}_k + \dot{C}_{D,k}} \tag{3.30}$$

where $\dot{C}_{D,k}$ are the exergy destruction costs and are calculated with the following equation [71]:

$$\dot{C}_{D,k} = c_f \dot{E}x_{D,k} \tag{3.31}$$

Here, $\dot{E}x_{D,k}$ is the exergy destruction. All the auxiliary equations determined together with the cost balance equations are given in Table 4.5.

The overall cost of the system ($\dot{C}_{system}$) can then be determined using the following equation [72]:

$$\dot{C}_{system} = \sum \dot{z}_k + \sum \dot{C}_{D,k} \tag{3.32}$$

Another crucial factor in the cost analysis is the system's unit cost of electricity produced ($\dot{C}_{electricity}$). The following equation is used to calculate the total cost of the electricity produced [72]:

$$\dot{C}_{electricity} = \frac{\dot{C}_{system}}{\dot{W}_{NET}} \tag{3.33}$$

Table 3.2. Energy and exergy balance equations in the triple-cycle power plant.

Component	Energy Balance Equation	Exergy Balance Equation
AC	$\dot{m}_1 h_1 + \dot{W}_{AC} = \dot{m}_2 h_2$	$\dot{E}_{D,AC} = (\dot{E}_1 - \dot{E}_2) + \dot{W}_{AC}$
SR	$\dot{m}_2 h_2 + \dot{Q}_{SR} = \dot{m}_3 h_3$	$\dot{E}_{D,SR} = (\dot{E}_2 - \dot{E}_3) + \dot{E}_{Q,Solar}$
CC	$\dot{m}_3 h_3 + \eta_{CC}\dot{m}_f \mathrm{LHV}_f = \dot{m}_4 h_4$	$\dot{E}_{D,CC} = \dot{E}_3 + \dot{E}_{Q,Fuel} - \dot{E}_4$
GT	$\dot{m}_4 h_4 = \dot{m}_5 h_5 + \dot{W}_{GT}$	$\dot{E}_{D,GT} = (\dot{E}_4 - \dot{E}_5) - \dot{W}_{GT}$
RBES Charging	$(m_5 h_5 - m_6 h_6) \times 3600 \times t_{charging} = m_{rock}\, c_{rock}(T_5 - T_0)$	$(\dot{E}_5 - \dot{E}_6) \times 3600 \times t_{charging} = m_{rock}\, c_{roc}$ $-T_0 \times \ln\left(\frac{T_5}{T_0}\right)) + \dot{E}_{D,charging} \times 3600 \times t_{c}$
RBES Discharging	$(m_8 h_8 - m_{10} h_{10}) \times 3600 \times t_{discharging} = m_{rock}\, c_{rock}(T_5 - T_0)$	$(\dot{E}_8 - \dot{E}_{10}) \times 3600 \times t_{discharging} + \dot{E}_{D,dis}$ $\times t_{discharging} = m_{rock}\, c_{rock}\,((T_5 - T_0) - T_{0}$
Blower	$\dot{m}_9 h_9 + \dot{W}_{blower} = \dot{m}_{10} h_{10}$	$\dot{E}_{D,blower} = (\dot{E}_9 - \dot{E}_{10}) + \dot{W}_{blower}$
Boiler	$\dot{m}_8(h_8 - h_9) = \dot{m}_{11}(h_{11} - h_{14})$	$\dot{E}_{D,Boiler} = \dot{E}_8 - \dot{E}_9 + \dot{E}_{14} - \dot{E}_{11}$
ST	$\dot{m}_{11} h_{11} = \dot{m}_{12} h_{12} + \dot{W}_{ST}$	$\dot{E}_{D,ST} = (\dot{E}_{11} - \dot{E}_{12}) - \dot{W}_{ST}$
Condenser	$\dot{m}_{12}(h_{12} - h_{13}) = \dot{m}_{19}(h_{20} - h_{19})$	$\dot{E}_{D,cond} = \dot{E}_{12} - \dot{E}_{13} + \dot{E}_{19} - \dot{E}_{20}$
Pump	$\dot{m}_{13} h_{13} + \dot{W}_{pump} = \dot{m}_{14} h_{14}$	$\dot{E}_{D,pump} = (\dot{E}_{13} - \dot{E}_{14}) + \dot{W}_{pump}$
HE	$\dot{m}_6(h_6 - h_7) = \dot{m}_{15}(h_{16} - h_{15})$	$\dot{E}_{D,HE} = \dot{E}_6 - \dot{E}_7 + \dot{E}_{15} - \dot{E}_{16}$
ORT	$\dot{m}_{16} h_{16} = \dot{m}_{17} h_{17} + \dot{W}_{ORT}$	$\dot{E}_{D,ORT} = (\dot{E}_{16} - \dot{E}_{17}) - \dot{W}_{ORT}$
ORC-Cond	$\dot{m}_{17}(h_{17} - h_{18}) = \dot{m}_{21}(h_{21} - h_{22})$	$\dot{E}_{D,ORC-Cond} = \dot{E}_{17} - \dot{E}_{18} + \dot{E}_{21} - \dot{E}_{22}$
ORP	$\dot{m}_{18} h_{18} + \dot{W}_{ORP} = \dot{m}_{15} h_{15}$	$\dot{E}_{D,ORP} = (\dot{E}_{18} - \dot{E}_{15}) + \dot{W}_{ORP}$

Table 3.3. Product and fuel exergy equations.

Component	Fuel Exergy Equation	Product Exergy Equation
AC	$\dot{W}_{AC}$	$\dot{E}_2 - \dot{E}_1$
SR	$\dot{E}_{Q,Solar}$	$\dot{E}_3 - \dot{E}_2$
CC	$\dot{E}_{Q,Fuel}$	$\dot{E}_4 - \dot{E}_3$
GT	$\dot{E}_4 - \dot{E}_5$	$\dot{W}_{GT}$
RBES Charging	$\dot{E}_5 - \dot{E}_6$	$m_{\text{rock}}\, c_{\text{rock}} \left((T_5 - T_0) - T_0 \times \ln\left(\frac{T_5}{T_0}\right)\right) / (3600 \times t_{\text{charging}})$
RBES Discharging	$m_{\text{rock}}\, c_{\text{rock}} \left((T_5 - T_0) - T_0 \times \ln\left(\frac{T_5}{T_0}\right)\right) / (3600 \times t_{\text{discharging}})$	$\dot{E}_8 - \dot{E}_{10}$
Blower	$\dot{W}_{blower}$	$\dot{E}_{10} - \dot{E}_9$
Boiler	$\dot{E}_8 - \dot{E}_9$	$\dot{E}_{11} - \dot{E}_{14}$
ST	$\dot{E}_{11} - \dot{E}_{12}$	$\dot{W}_{ST}$
Condenser	$\dot{E}_{12} - \dot{E}_{13}$	$\dot{E}_{20} - \dot{E}_{19}$
Pump	$\dot{W}_{pump}$	$\dot{E}_{14} - \dot{E}_{13}$
HE	$\dot{E}_6 - \dot{E}_7$	$\dot{E}_{16} - \dot{E}_{15}$
ORT	$\dot{E}_{16} - \dot{E}_{17}$	$\dot{W}_{ORT}$
ORC-Cond	$\dot{E}_{17} - \dot{E}_{18}$	$\dot{E}_{22} - \dot{E}_{21}$
ORP	$\dot{W}_{ORP}$	$\dot{E}_{15} - \dot{E}_{18}$

Table 3.4. Cost balance equations for the system elements.

Component	Cost Flow Equations	Auxiliary Equations	Investment Cost
AC	$\dot{C}_1 + \dot{C}_{AC} + \dot{Z}_{AC} = \dot{C}_2$	$c_1 = 0$	$\dot{Z}_{AC} = (71.1 \times \dot{m}_{air}/0.9 - \eta_{comp})(p_2/p_1)\text{Ln}(p_2/p_1)$ [73]
SR	$\dot{C}_2 + \dot{Z}_{hel} = \dot{C}_3$	$c_2 = c_3$	$\dot{Z}_{Hel} = 126 * A_{hel}$
CC	$\dot{C}_3 + \dot{C}_{fuel} + \dot{Z}_{CC} = \dot{C}_4$	$c_3 = c_4$ $c_f = 12$	$\dot{Z}_{CC} = (46.08 \times \dot{m}_{air}/0.996 - (p_4/p_2))(1 + \exp(0.018 \times T_4 - 26.4))$ [73]
GT	$\dot{C}_4 + \dot{Z}_{GT} = \dot{C}_5 + \dot{C}_{GT}$	$c_4 = c_5$ $c_{AC} = c_{GT}$	$\dot{Z}_{GT} = (479.34 \times \dot{m}_4/0.92 - \eta_{GT})\text{Ln}(p_4/p_5)\,(1 + \exp(0.036 \times T_4 - 54.4))$ [73]
RBES	$\dot{C}_5 + \dot{C}_{10} + \dot{Z}_{RBES} = \dot{C}_6 + \dot{C}_8$	$c_5 = c_6$	$\dot{Z}_{RBES} = 1380 * V_{rock}^{0.4}$ [51]
Blower	$\dot{C}_9 + \dot{C}_{Blower} + \dot{Z}_{Blower} = \dot{C}_{10}$	$c_{blower} = c_{GT}$	$\dot{Z}_{Blower} = 91562 * (\dot{W}_{Blower}/455)^{0.67}$ [74]
Boiler	$\dot{C}_8 + \dot{C}_{14} + \dot{Z}_{Boiler} = \dot{C}_9 + \dot{C}_{11}$	$c_8 = c_9$	$\dot{Z}_{Boiler} = (1/1.12) * 180 * \dot{Q}_{Boilr}$ [74]
ST	$\dot{C}_{11} + \dot{Z}_{ST} = \dot{C}_{12} + \dot{C}_{ST}$	$c_{12} = c_{11}$	$\dot{Z}_{ST} = 6000\, \dot{W}_{ST}^{0.7}$ [75]
Condenser	$\dot{C}_{12} + \dot{C}_{19} + \dot{Z}_{Condenser} = \dot{C}_{13} + \dot{C}_{20}$	$c_{12} = c_{13}$ $c_{10} = 0$	$\dot{Z}_{Condenser} = 1773\, \dot{m}_{steam}$ [76]
Pump	$\dot{C}_{13} + \dot{C}_{Pump} + \dot{Z}_{pump} = \dot{C}_{14}$	$c_{Pump} = c_{ST}$	$\dot{Z}_{Pump} = 2100\, \dot{W}_{pump}^{0.26} (1 - \eta_{Pump}/\eta_{Pump})^{0,5}$ [76]
HE	$\dot{C}_6 + \dot{C}_{15} + \dot{Z}_{HE} = \dot{C}_7 + \dot{C}_{16}$	$c_7 = 0$	$\dot{Z}_{HE} = 235 * \dot{Q}_{HE}$ [69]
ORT	$\dot{C}_{16} + \dot{Z}_{ORT} = \dot{C}_{17} + \dot{C}_{ORT}$	$c_{16} = c_{17}$	$\dot{Z}_{ORT} = (479.3\, \dot{m}_{16}/0.92 - \eta_{ORT})\text{Ln}(p_{16}/p_{17})\,(1 + \exp(0.036 \times T_{16} - 54.4))$ [64]
ORC-Cond	$\dot{C}_{17} + \dot{C}_{21} + \dot{Z}_{ORC-Cond} = \dot{C}_{18} + \dot{C}_{22}$	$c_{17} = c_{18}$ $c_{21} = 0$	$\dot{Z}_{ORC-Cond} = 1773\, \dot{m}_{17}$ [76]
ORP	$\dot{C}_{18} + \dot{C}_{ORP} + \dot{Z}_{ORP} = \dot{C}_{14}$	$c_{ORP} = c_{ORT}$	$\dot{Z}_{ORP} = 2100\, \dot{W}_{ORP}^{0.26} (1 - \eta_{ORP}/\eta_{ORP})^{0,5}$ [76]

PART 4

RESULTS AND DISCUSSIONS

The findings obtained from the energy, exergy, and cost balance equations applied to each solar-based triple combined cycle component are discussed in this chapter. In addition, the exergy destruction ($\dot{E}x_x$), and capital investment cost ($\dot{z}_k$)for the system components are performed. A parametric study is also executed to study the influences of varying significant parameters such as ambient temperature, pressure ratio, compressor isentropic efficiency, turbine isentropic efficiency, and gas turbine inlet temperature. Moreover, the variation in the system's power and electricity cost rate each month is explained. The thermodynamic model of the solar-based triple combined cycle in this research has been validated with the results of published work by Öztürk et al. [36], as illustrated in Figure 4.1. It is clear that the findings of this investigation are comparable and close to those found in the literature. Table 4.1 presents the computed and assumed properties for all state points.

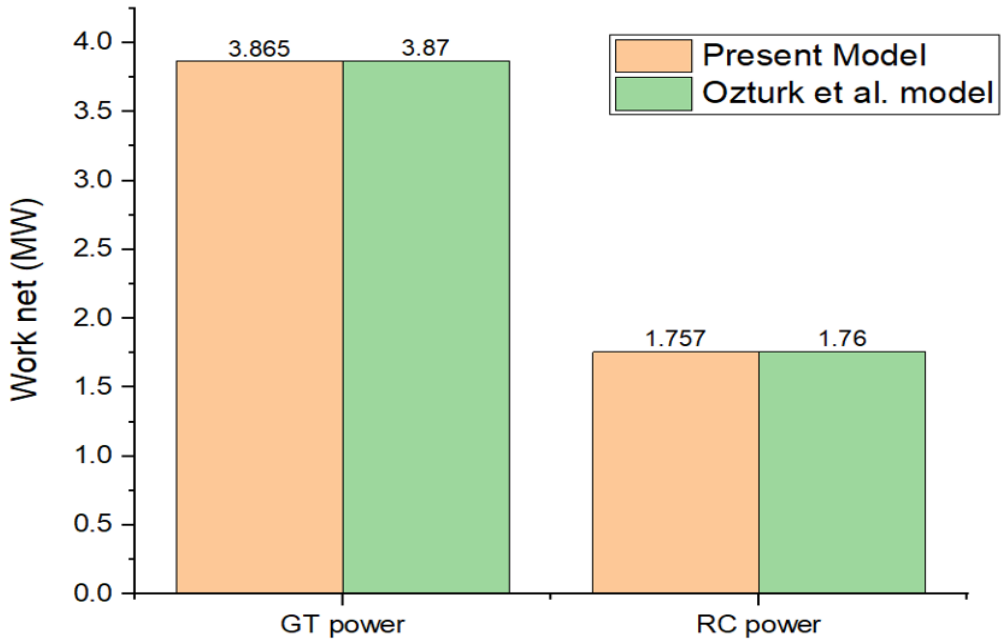

Figure 4.1. Validation of the present thermodynamic model with published work by Öztürk et al. [36].

Table 4.1. Thermodynamic Properties for each state for the solar-based triple combined cycle at the optimum condition.

State	$\dot{m}$ (kg/s)	P (bar)	T (℃)	h (kJ/kg)	S (KJ/kg. K)	x (-)	$\dot{E}$ (MW)
1	51.76	298	100	298.4	5.699		0
2	51.76	715.4	1620	730.2	5.8		20.79
3	51.76	1178	1620	1252	6.36		39.14
4	51.76	1273	1620	1364	6.452		43.54
5	51.76	735	106.6	751.3	6.61		9.382
6	51.76	382.3	100	383.4	5.95		0.5249
7	51.76	336.1	100	336.7	5.82		0.1148
8	37.35	725	107	740.5	6.594		6.544
9	37.35	343.2	107	343.9	5.822		0.332
10	37.35	375.3	140	376.3	5.835		1.397
11	4.909	705	5000	3274	6.76	100	6.204
12	4.909	333	19.81	2435	7.39	0.9265	1.166
13	4.909	333	19.81	250.6	0.8294	0	0.03924
14	4.909	333.2	5000	256.2	0.8311	−100	0.06437
15	6.585	321.1	1700	317.7	1.387	−100	0.3621
16	6.585	370.3	1700	684.6	2.413		0.7639
17	6.585	340	635.7	657.5	2.451	100	0.5118
18	6.585	320.2	635.7	315.2	1.386	0	0.3484
19	256.5	298	100	104.2	0.3651		0
20	256.5	308	100	146	0.5031		0.1766
21	53.92	298	100	104.2	0.3651		0
22	53.92	308	100	146	0.5031		0.03713

4.1. EXERGY ANALYSIS

The exergy analysis findings for the solar-based triple combined cycle components under optimum operating conditions are shown in Table 4.2 and Figure 4.2. When the temperature differences are larger, more exergy destruction occurs. As a result, the solar receiver, which experiences the largest temperature difference, has the highest rates of exergy destruction (7.301 MW). The gas turbine, and CC rank second and third, respectively. Table 4.2 and Figure 4.2 reveal the exergy destruction ratio for the main component of the solar-based triple combined cycle. It is evident that the SR, GT, and CC are responsible for 43.34%, 14.49%, and 9.63% of the total exergy destruction, respectively. The significant exergy destruction of the GT is brought on by the impact of a large volume of hot air against the turbine blades positioned in the shaft. In descending order, the RBES, AC, condenser, and ST also contribute significantly to the total exergy destruction rate. The RBES contributes 9.61% of the

total exergy destruction, making it the fourth-highest contributor. The high exergy loss in the RBES is caused by the process of charging and discharging, which creates many irreversible situations. Figure 4.2 does not show the exergy destruction ratio of the components such as pumps, condensers, and HE due to their marginal values. Table 4.2, however, presents the exergy efficacy of all the system's components. The boiler and HE show the highest exergy efficiency of 98.0%.

Table 4.2. Exergy analysis for each component of the solar-based triple combined cycle.

Component	$\dot{E}_{input}$ **(MW)**	$\dot{E}_{output}$ **(MW)**	$\dot{E}_{destruction}$ **(MW)**	$\dot{E}_{destruction}$ **(%)**	**Exergy efficiency (%)**
AC	22.35	20.97	1.561	9.27	93.01
SR	25.65	18.35	7.301	43.34	71.54
CC	6.027	4.405	1.622	9.63	73.1
GT	34.16	31.72	2.441	14.49	92.85
RBES Charging	8.86	7.32	1.538	9.126	82.64
RBES Discharging	5.23	5.147	0.0816	0.4845	98.44
RBES	14.09	12.47	1.619	9.61	
Blower	1.21	1.065	0.145	0.86	88.03
Boiler	6.212	6.14	0.072	0.43	98.8
ST	5.038	4.117	0.921	5.47	81.72
Condenser	1.127	0.1766	0.951	5.64	15.67
Pump	0.0276	0.02513	0.00247	0.0147	91.06
Heat exchanger	0.41	0.4018	0.008	0.05	98
ORT	0.2521	0.1718	0.0739	0.44	70.1
ORC-Cond	0.1633	0.03713	0.1262	0.75	22.73
ORP	0.0168	0.01368	0.003	0.018	81.43
Total			16.85		

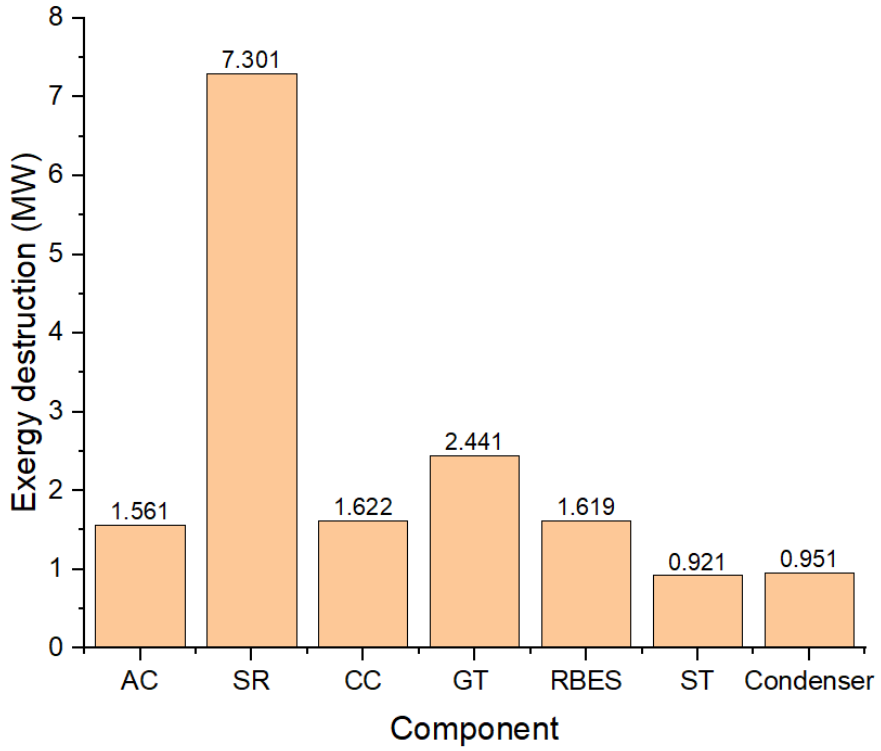

Figure 4.2. Destruction rates of the exergy for the system components.

4.2. EXERGO-ECONOMIC ANALYSIS

Table 4.3 presents a summary of the findings from the exergo-economic modelling. It presents the exergy rate ($\dot{E}$), cost per unit exergy rate (c), and cost rate ($\dot{C}$) for each state. The important exergo-economic characteristics are assessed based on the cost-per-unit exergy rates of the various parts of the system. The exergo-economic parameters for the solar-based triple combined cycle are listed in Table 4.4. The solar receiver has the highest capital cost rate of all the components at 105.77 $/h of the capital cost rate, and the ST has the next element at 53.12 $/h. The CC, AC, boiler, and GT also have relatively high capital cost rates. The RBES, HE, and ORT also contribute to the capital costs of the plant, with rates ranging from 3.386 $/h to 10.08 $/h. The capital cost rates for the other parts of the system are low.

Table 4.4 shows the cost rate for exergy destruction, which is a crucial factor in exergo-economic analysis since, in some cases, it is much higher than the capital cost rate. It can be shown that the CC has the highest cost rate of exergy destruction ($\dot{C}_D$) at 51.82 $/h. The GT has a rather high $\dot{C}_D$ value and is the second most important part

after the CC. It can also be shown that the capital cost rate of the system is much higher than the total cost rate of exergy destruction.

In exergo-economic analysis, the parts with the highest $\dot{Z}_k + \dot{C}_D$ values are seen as the most important from a cost standpoint. Table 4.4 shows that the SR has the highest value of $\dot{Z}_k + \dot{C}_D$, followed by the ST. The table also demonstrates that the exergo-economic factor for the solar-based triple combined cycle is exceptionally high (62.9%).

Table 4.3. Cost rates and cost rates per unit of exergy of streams in the solar-based triple combined cycle.

State	$\dot{E}$ (MW)	$\dot{C}$ ($/h)	c ($/GJ)
1	0	0	0
2	20.79	119.8	1.601
3	39.14	225.6	1.601
4	43.54	418.3	2.668
5	9.382	90.13	2.668
6	0.5249	5.043	2.668
7	0.1148	0	0
8	6.544	103.9	4.411
9	0.332	5.271	4.411
10	1.397	18.53	3.685
11	6.204	144.6	6.473
12	1.166	27.18	6.473
13	0.03924	0.9144	6.473
14	0.06437	2.494	10.77
15	0.3621	15.33	11.76
16	0.7639	31.16	11.33
17	0.5118	20.87	11.33
18	0.3484	14.21	11.33
19	0	0	0
20	0.1766	26.4	41.53
21	0	0	0
22	0.03713	6.844	51.21

Table 4.4. Exergo-economic results of components of the solar-based triple combined cycle.

Component	c_f ($/GJ)	c_p ($/GJ)	$\dot{C}_D$ ($/h)	$\dot{Z}_K$ ($/h)	$\dot{Z}_K + \dot{C}_D$ ($/h)	r (%)	f (%)
AC	0.9537	1.6	5.36	43.07	48.43	67.86	88.93
SR	-	1.601	-	105.8	105.8	-	100
CC	8.875	12.15	51.82	0.17	51.99	36.94	0.319
GT	2.67	2.99	23.45	13.14	36.59	12.01	35.9
RBES	1.678	1.902	9.78	0.3	10.08	13.38	2.96
Blower	2.99	3.46	1.559	0.242	1.801	15.72	13.45
Boiler	4.41	6.43	1.147	43.443	44.59	45.73	97.43
ST	6.473	10.06	21.46	31.66	53.12	55.37	59.59
Condenser	6.473	41.53	22.15	0.14	22.29	541.5	0.6078
Pump	10.06	17.47	0.089	0.581	0.67	73.67	86.67
HE	3.415	10.94	0.1023	10.7877	10.89	220.4	99
ORT	11.33	16.61	3.014	0.372	3.386	46.58	10.98
ORC-Cond	11.33	51.21	5.148	0.182	5.33	352	3.41
ORP	16.61	32.08	0.1865	0.1135	0.3	93.16	37.66
Total System			145.3	247.2	392.5		62.9

4.3. OPERATION PARAMETERS ANALYSIS

4.3.1. Effects of Ambient Temperature

Figures 4.3 and 4.4 show the effects of ambient temperature (T_1) on the values of the work net, the system's electricity cost rate, and the overall system efficiencies. It is apparent from the figures that $\dot{W}_{net}$, $\dot{C}_{\text{electricity}}$, η_I, and η_{II} decrease with an increase in the ambient temperature. When T_1 increases, h_2 increases, and the power consumed by AC increases, too. Part of $\dot{W}_{net}$ is used to operate the compressor and the increase in $\dot{W}_{AC}$ has a negative effect in the work net and overall system efficiencies. Figure 4.3 demonstrates that as T_1 increases from 288 K to 310 K, $\dot{W}_{net}$ decreases from 13,782 kW to 12,229 kW. The findings also indicate that decreasing the output power of the solar-based triple combined cycle leads to a very slight decrease in the system's total and electrical cost rate values. The total capital investment, maintenance, and operation cost rates for the entire cycle decrease, resulting in a steady decrease in the specific cost per unit of electricity produced. By increasing T_1 from 290 K to 312 K, $\dot{C}_{\text{electricity}}$ decreases from 32.26 $/MWh to 31.28 $/MWh. In addition, η_I from the solar-based triple combined cycle decreases from 38.44% to 36.66%, and η_{Il} falls from 42.1% to 39.57%, as seen in Figure 4.4.

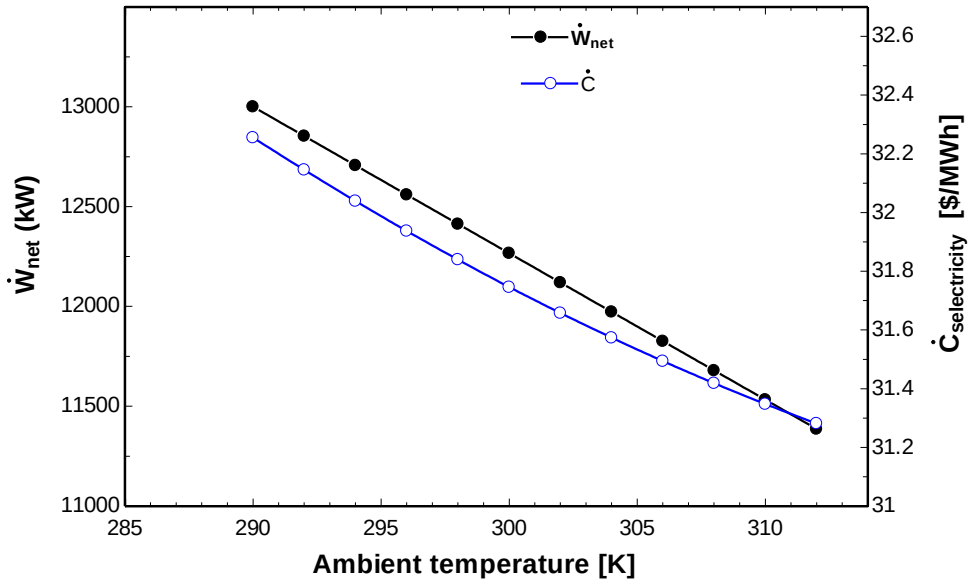

Figure 4.3. Variation of work net and electricity cost rate of the system according to the ambient temperature.

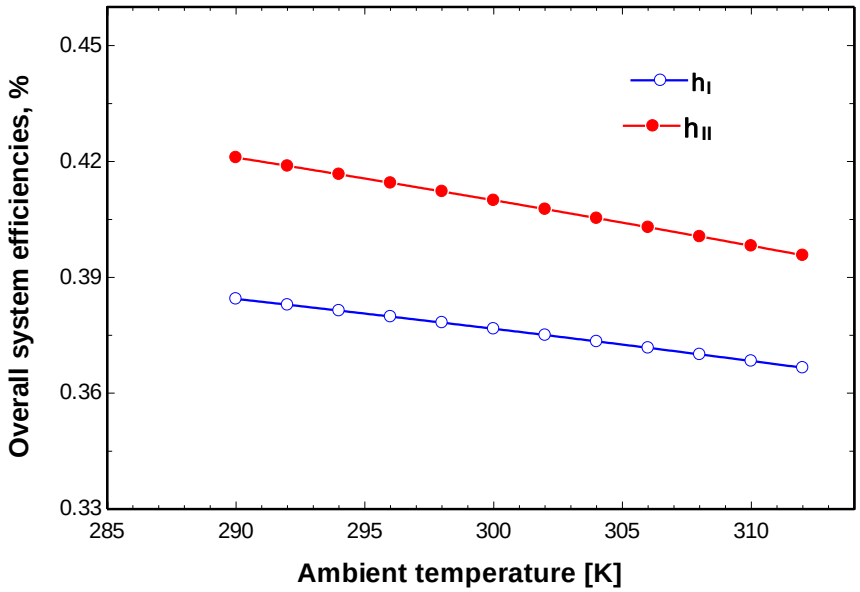

Figure 4.4. Variation of overall system efficiencies according to the ambient temperature.

4.3.2. Effects of Pressure Ratio

Figure 4.5 illustrates the effects of pressure ratio (PR) on the power generation values in the overall system, BC, RC and ORC. Because of a constant inlet air flow rate, the work of the air compressor ($\dot{W}_{AC}$) and gas turbine ($\dot{W}_{GT}$) increases with the increase in PR. The effect of these parameters will cause power generation in BC to increase first and then decrease with an increasing PR. $\dot{W}_{ORC}$ remains constant for all values of PR.

When PR increases, h_2 increases and h_5 decreases, which leads to increased work input to AC and work output from GT. At high PR values, the air temperature at the end of the GT decreases and leads to a reduction in $\dot{W}_{RC}$.

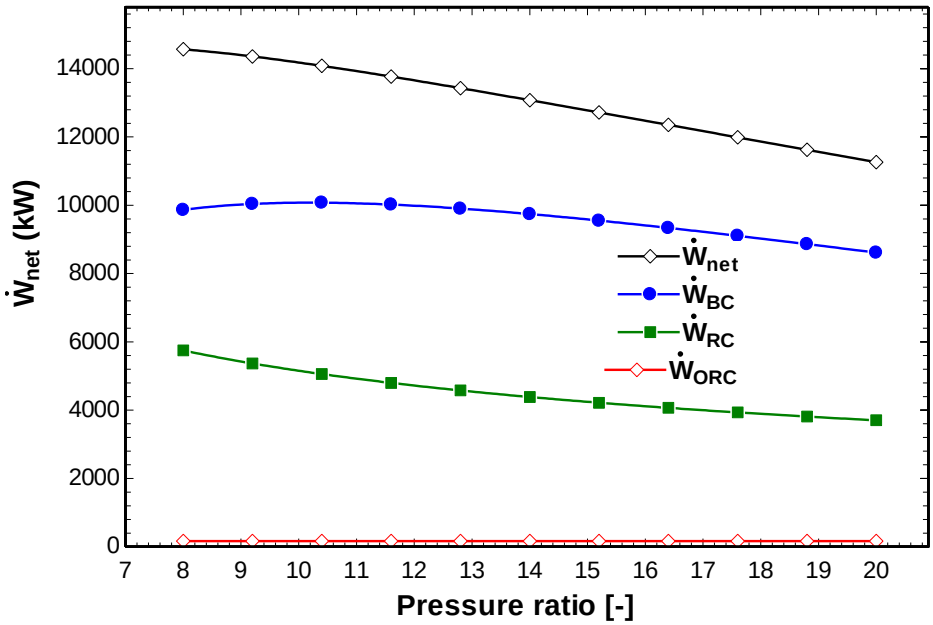

Figure 4.5. Power generation values in the overall system, BC, RC and ORC, according to the pressure ratio.

The impacts of the pressure ratio on the values of the work net, the system's electricity cost rate, and the First and Second Law overall efficiencies of the system are shown in Figures 4.6 and 4.7. The finding demonstrates that when PR increases, the $\dot{W}_{net}$ of the system decreases as a result of the increase in the work of the air compressor. $\dot{W}_{net}$ drops from 14,556 kW to 12,261 kW (a decrease of approximately 3,305 kW) when PR increases from 8 to 20, as seen in Figure 4.6. Increasing PR up to 16.4 reduces the system's electricity cost rate from 36.21 \$/h to 31.85 \$/h, which is due to the reduction of $\dot{W}_{net}$ and the fuel input rate. When PR exceeds 16.4, the system's electricity cost rate. This is mostly due to the extreme decline in the $\dot{W}_{net}$ of the system.

Figure 4.7 illustrates that when PR rises, system efficiency improves until it peaks, after which it drops. At high values of PR, $\dot{W}_{net}$ reduces and negatively affects the overall system efficiencies. The maximum η_I and η_{II} were obtained at 14 bars (37.94% and 41.68%, respectively).

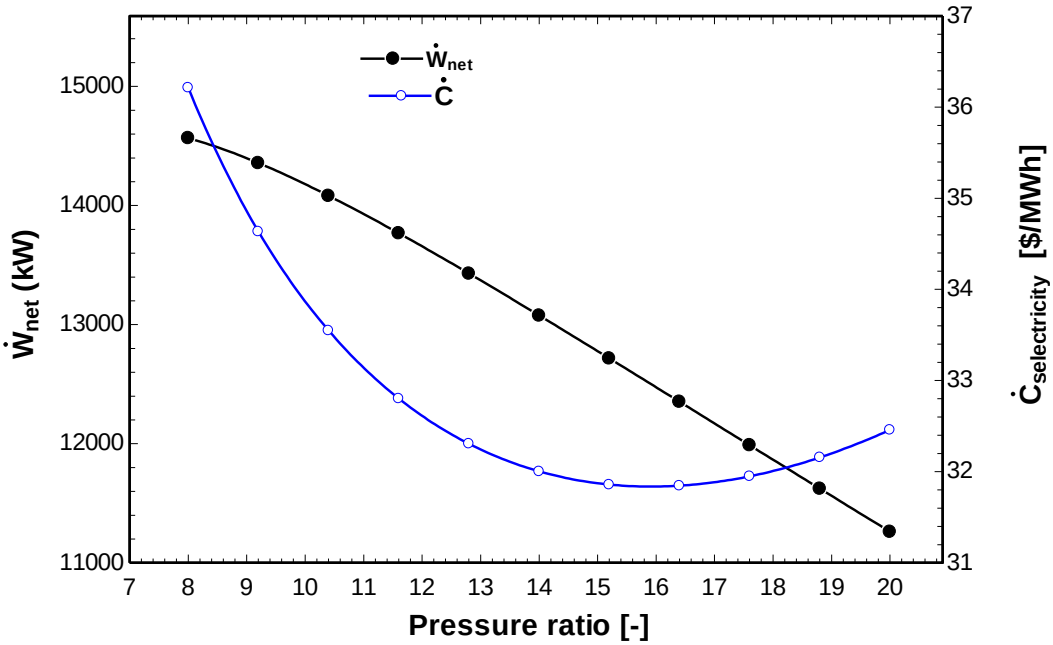

Figure 4.6. Variation of work net and electricity cost rate of the system according to the pressure ratio.

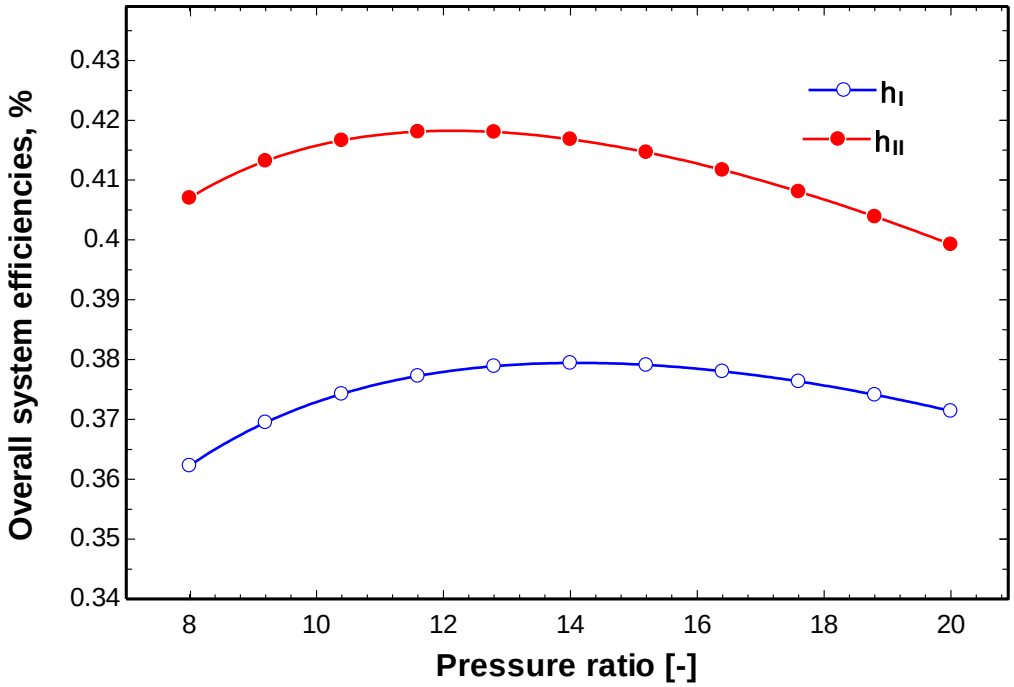

Figure 4.7. Variation of overall system efficiencies according to the pressure ratio.

4.3.3. Effects of Air Compressor Isentropic Efficiency

Figures 4.8 and 4.9 present the influence of air compressor isentropic efficiency (η_{AC}) on the values of the work net, the system's electricity cost rate, and the overall system

efficiencies. The figures illustrate that a rise in η_{AC} increases the $\dot{W}_{net}$ and enhances the First and Second Law efficiencies of the system. The inlet air flow rate remains constant and the power consumption by the air compressor decreases when η_{AC} increases. A rise in η_{AC} from 75% to 88% raises $\dot{W}_{net}$ from 9,731 kW to 13,249 kW (an increase of 3,518 kW), as shown in Figure 4.8. This finding shows that a decrease in the system's electricity cost rate can be achieved by increasing η_{AC} from 75% to around 83%. However, the system's electricity cost rate rises as η_{AC} exceeds 83%. $\dot{C}_{\text{electricity}}$ decreases significantly from 34.64 \$/MWh until it reaches a minimum value of 31.78 \$/MWh at η_{AC} of 83%, before rising to 36.54 \$/MWh at η_{AC} of 88%.

Figure 4.9 shows that better cycle efficiency in both the First and Second Laws can be achieved by increasing η_{AC}. According to this figure, when η_{AC} changes from 75% to about 88%, η_I increases from 32.29% to approximately 39.7%, and η_{II} rises from 34.7% to 53.5%.

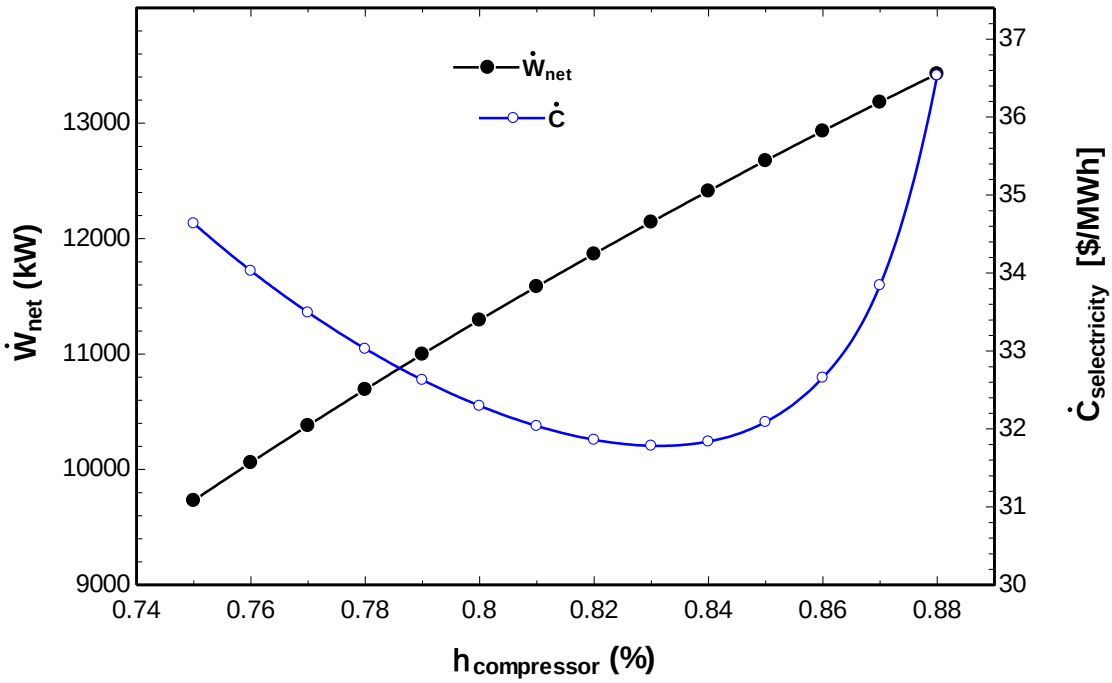

Figure 4.8. Variation of work net and electricity cost rate of the system according to air compressor isentropic efficiency.

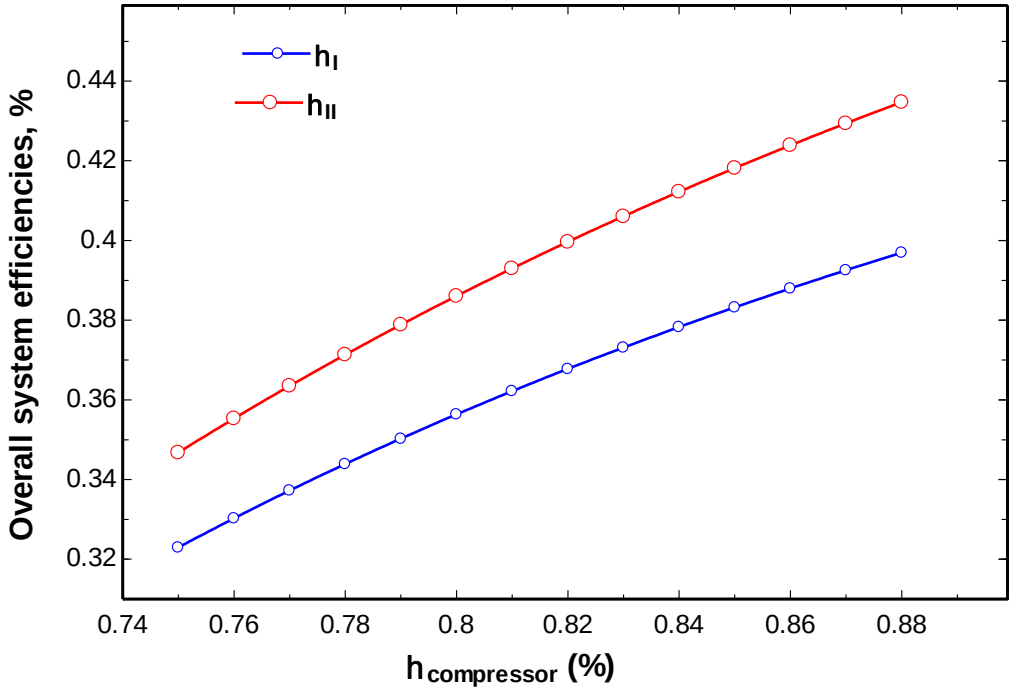

Figure 4.9. Variation of overall system efficiencies according to the air compressor isentropic efficiency.

4.3.4. Effects of Gas Turbine Isentropic Efficiency

The effect of the gas turbine isentropic efficiency (η_{GT}) on work net values, the system's electricity cost rate, and First and Second Law overall efficiencies of the system are shown in Figures 4.10 and 4.11. The graph depicts the effect of increasing the η_{GT} on the system's performance and cost. Boosting the gas turbine's isentropic efficiency improves $\dot{W}_{net}$, and system's First and Second Law efficiencies by reducing fuel consumption and the exergy destruction rate. Moreover, the main reason for this enhancement is that the work produced by GT will increase if η_{GT} is raised. The system's electricity cost rate is reduced due to enhanced gas turbine isentropic efficiency. Figure 4.10 illustrates that as η_{GT} increases from 79% to 90%, $\dot{W}_{net}$ increases from 10,649 kW to 13,859 kW (an increase of 3,210 kW). The lowest electricity cost rate of the system drops from 38.59 $/MWh to 28.7 $/MWh; η_I of the solar-based triple combined cycle rises from 32.59% to 42.24%, and η_{Il} rises from 35.51% to 46.03%, as seen in Figure 4.11.

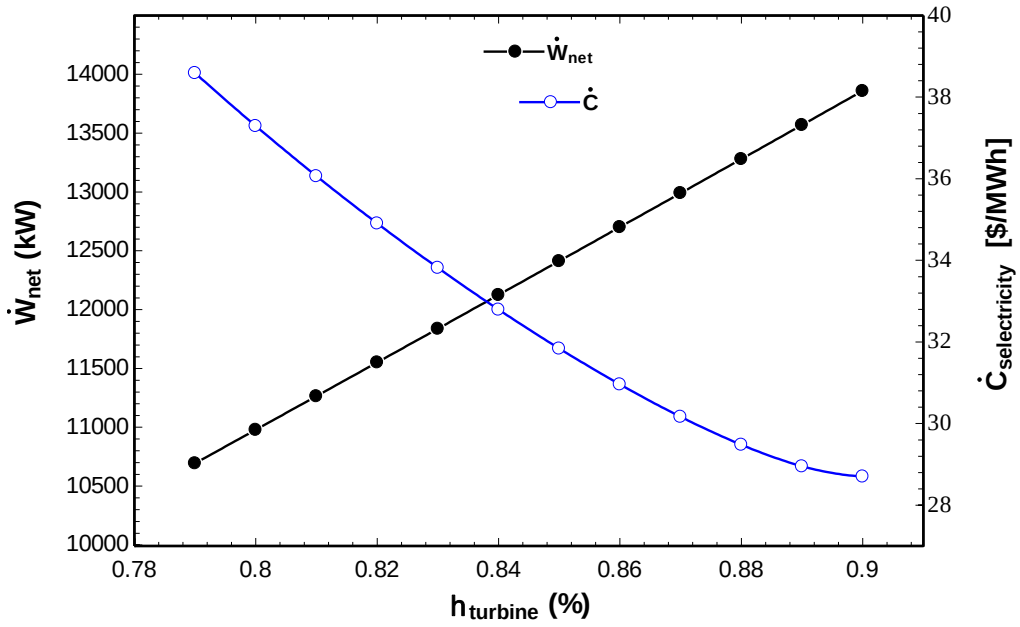

Figure 4.10. Variation of work net and electricity cost rate of the system according to the gas turbine isentropic efficiency.

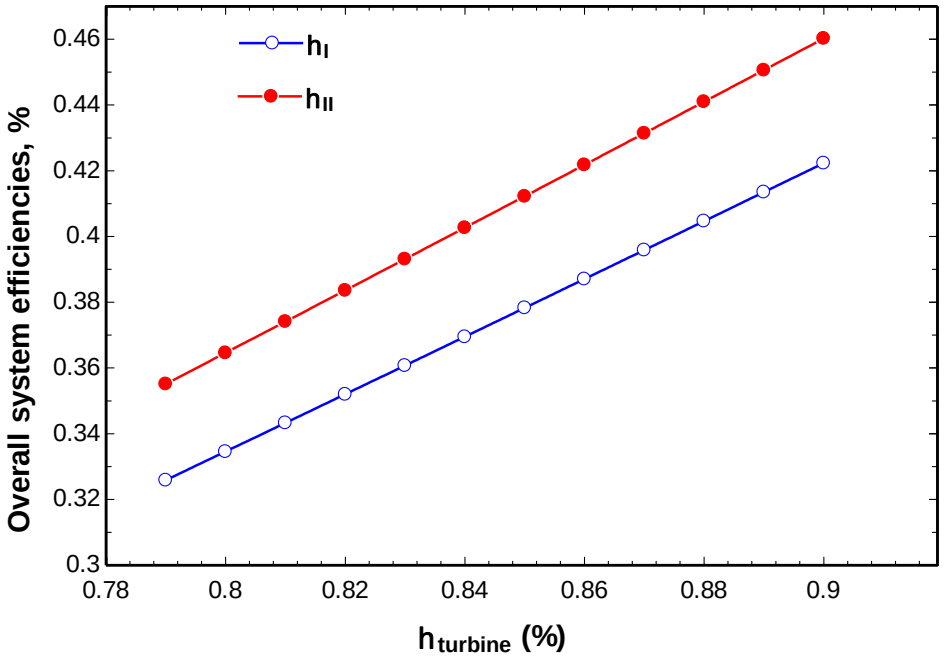

Figure 4.11. Variation of overall system efficiencies according to the gas turbine isentropic efficiency.

The impacts of the gas turbine inlet temperature (T_4) on the values of the work net, the electricity cost rate of the system, and the overall First and Second Law efficiencies of the system are shown in Figures 4.12 and 4.13. According to these figures, increasing the gas turbine inlet temperature enhances the work net of the system, as well as overall

efficiencies. At 1,200 K, the system has the highest First and Second Law efficiencies of 42.88% and 48.24%, respectively. An increase in the turbine inlet temperature leads to an increase in the energy and exergy inputs into the gas turbine. On the other hand, by increasing turbine inlet temperature, energy storage in the RBES increases remarkably, which leads to an increase in the overall efficiencies and an increase in the $\dot{W}_{net}$ of the system. When T4 increases from 800 K to 1,000 K, $\dot{W}_{net}$ rises from 5,702 kW to 19,382 kW (an increase of 15,864 kW). These findings also show that the gas turbine inlet temperature has a significant impact on the system's electricity cost rate. Figure 4.12 shows that when the gas turbine inlet temperature rises, the system's power cost rate drops to a minimum and then rises again. The results also indicate that 1,160 K was the optimal GTIT temperature. $\dot{C}_{\text{electricity}}$ of the system was 31.49 $/MWh at the GTIT optimum value.

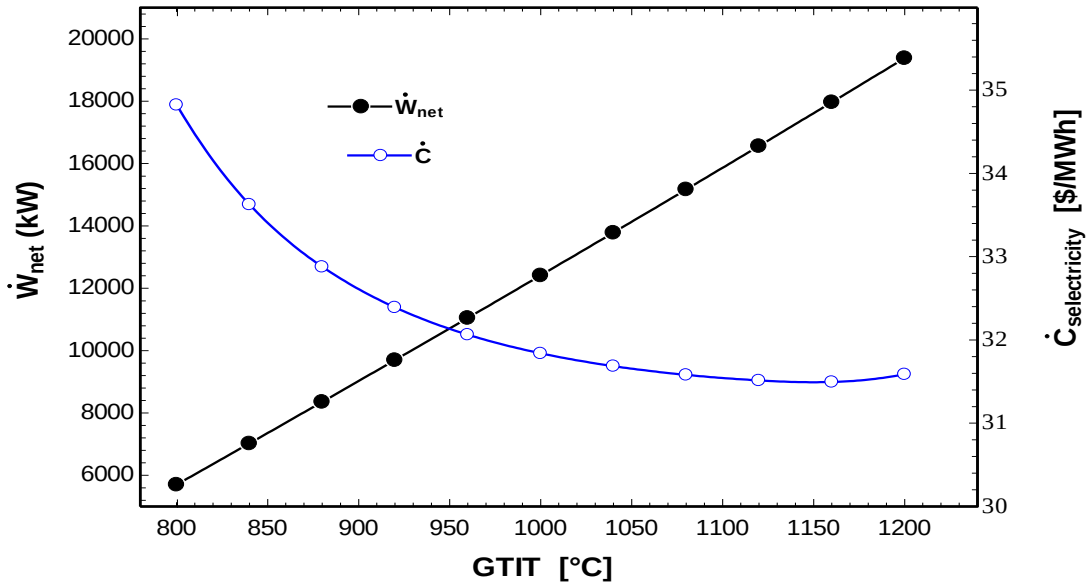

Figure 4.12. Variation of work net and electricity cost rate of the system according to the gas turbine inlet temperature.

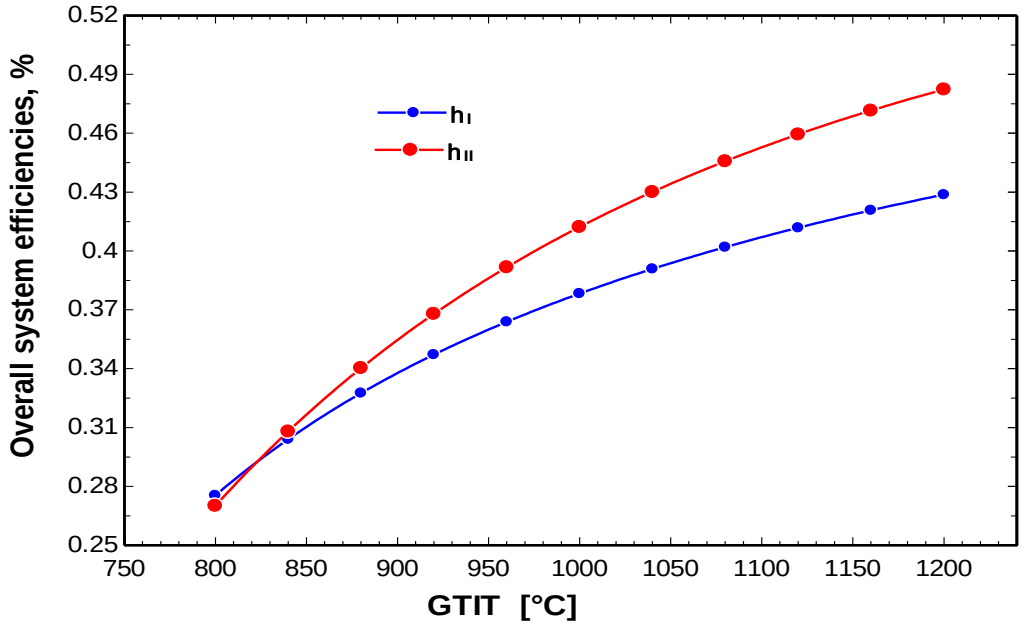

Figure 4.13. Variation of overall system efficiencies according to the gas turbine inlet temperature.

4.4. PERFORMANCE OF THE SYSTEM

Figure 4.14 shows the variation of Solar and Fuel shares under each month. The results illustrate that the heat provided by the sun increases in summer due to an increase in solar radiation intensity (with 85% of heat being provided by the sun in June). The system only needs a large amount of heat supplied from fuel in the winter (as only 43% of heat is provided by the sun in December).

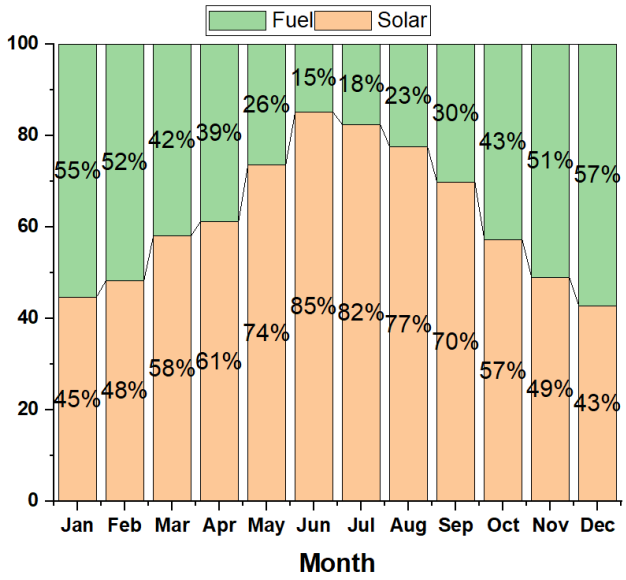

Figure 4.14. Variation of Solar and Fuel shares under each month.

The monthly variation of the system's work net is shown in Figure 4.15. The findings indicate that the maximum power produced by the system occurs in January due to the increased heat supplied by the fuel. The reason is that the quality of the energy produced by the fuel is higher than that produced by the sun, and the power produced by the gas turbine cycle is enhanced in a cold environment. The results show that the system produced 13,545 kW in January, whereas 11,567 kW of power was produced in July.

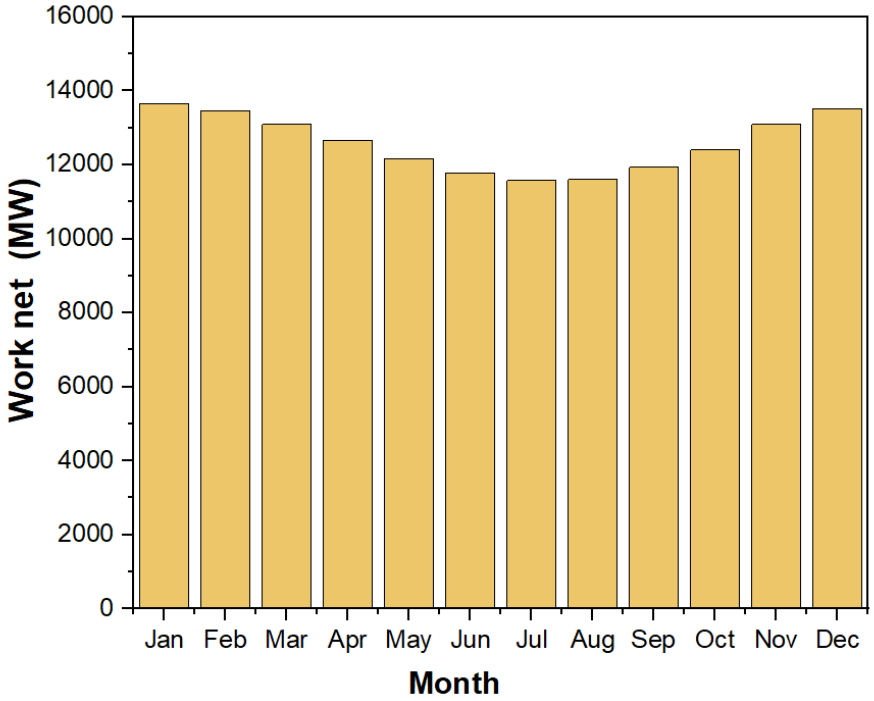

Figure 4.15. Variation of the system's work net under each month.

The monthly variation of the system's electricity cost rate is presented in Figure 4.16. The results revealed that the system's electricity cost rate is higher in the winter than in the summer, which is due to most of the system's power produced in the summer being produced from the sun's heat, which is cost free. The results show that the system's electricity cost rate is 31.5 $/MWh in June, whereas it reaches 49.54 $/MWh in December.

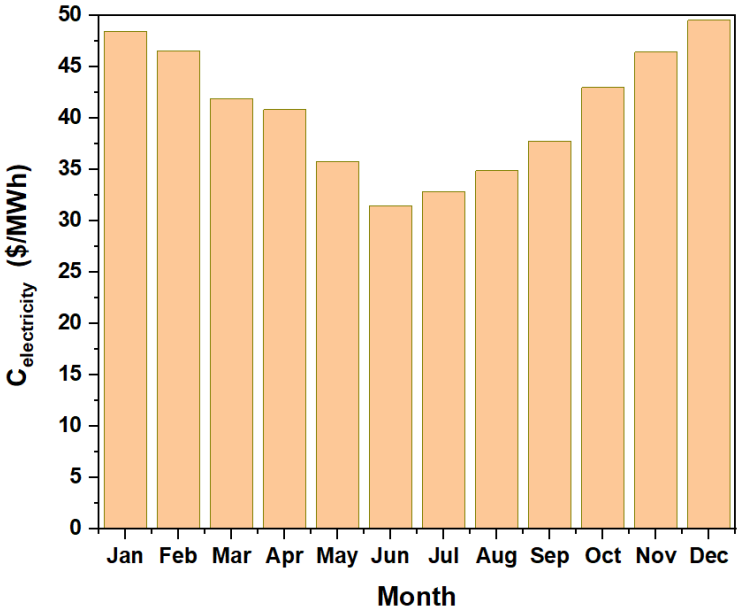

Figure 4.16. Variation of the system's electricity cost rate under each month.

PART 5

CONCLUSION AND FUTURE WORK

In this study, a unique solar-based triple combined cycle was designed and thermodynamic and exergo-economic analyses were carried out. In the system under investigation, electricity production was obtained by the CSP plant, which is selected for the city of Tikrit in Iraq. In the solar-based triple combined cycle, gas turbine, steam Rankin, and organic Rankine cycles produce power using the thermal energy generated from the concentration solar collectors. The effects of important variables such as ambient temperature, pressure ratio, compressor isentropic efficiency, turbine isentropic efficiency, and gas turbine inlet temperature were investigated on the system's performance and cost. Several conclusions can be drawn as follows:

- In the solar-based triple combined cycle, the maximum power output from the system can generate 13,545 kW in January, and the minimum power output is 11,567 kW, obtained in July.
- The system's electricity cost rate is more expensive in the winter than in the summer. The system's electricity cost rate was 31.5 $/MWh in June, whereas it reached 49.54 $/MWh in December.
- The RBES is charged by the hot exhaust gas from the gas turbine cycle for 10 hours, and it discharges it to operate the steam cycle for 14 hours.
- The exergo-economic factor (f_k) is an important parameter to be calculated in the exergy economics analysis. The solar-based triple combined cycle has an extraordinarily high exergo-economic factor. It reaches 62.9%, which will encourage the Iraqi government to build this power plant.
- When the systems were examined regarding exergy destruction cost, the total cost was found to be 145.3 $/h. The highest exergy destruction cost was found in the combustion chamber at 51.82 $/h. The lowest exergy destruction cost was calculated at 0.089 $/h for the pump.

- The ambient temperature significantly affects the system's performance and cost, which should be considered during system design.
- Increasing the pressure ratio reduces the system's cost but negatively impacts the power output.
- Increasing the air compressor isentropic efficiency enhances the system's power output and efficiencies, but the system's electricity cost rate reduces to an optimum point and then increases.
- Increasing the gas turbine isentropic efficiency and gas turbine inlet temperature significantly improves the system's performance and efficiencies and simultaneously reduces the system's electricity cost rate.

Different power plant cycles can be developed in future studies with other renewable energy sources. Optimization studies can be carried out for newly developed techniques, and analyses can be expanded on the optimum inclusion of resources in the system.

REFERENCES

1. Ma, Z., Glatzmaier, G. C., and Kutscher, C. F., "Thermal energy storage and its potential applications in solar thermal power plants and electricity storage", ***ASME 2011 5th International Conference On Energy Sustainability, ES 2011***, (PARTS A, B, AND C): 447–456 (2011).

2. Strielkowski, W., Tarkhanova, E., Tvaronavi˘, M., and Petrenko, Y., "Renewable Energy in the Sustainable Development of Electrical", ***Energies***, 14(24), 82: 1–24 (2021).

3. DELIBAS, H. M. and ERHAN KAYABASI, "ENERGY, ENVIRONMENT AND ECONOMY ASSESSMENT OF WASTE HEAT RECOVERY TECHNOLOGIES IN MARINE INDUSTRY", ***Materials And Engineering Technology***, 002 (2021): 39–45 (2019).

4. Kuravi, S., Trahan, J., Goswami, D. Y., Rahman, M. M., and Stefanakos, E. K., "Thermal energy storage technologies and systems for concentrating solar power plants", ***Progress In Energy And Combustion Science***, 39 (4): 285–319 (2013).

5. Alnaimat, F. and Rashid, Y., "Thermal energy storage in solar power plants: A review of the materials, associated limitations, and proposed solutions", ***Energies***, 12 (21): (2019).

6. Kuravi, S., Goswami, Y., Stefanakos, E. K., Ram, M., Jotshi, C., Pendyala, S., Trahan, J., Sridharan, P., Rahman, M., and Krakow, B., "Thermal Energy Storage for Concentrating Solar Power Plants", ***Technology & Innovation***, 14 (2): 81–91 (2012).

7. N'Tsoukpoe, K. E., Liu, H., Le Pierrès, N., and Luo, L., "A review on long-term sorption solar energy storage", ***Renewable And Sustainable Energy Reviews***, 13 (9): 2385–2396 (2009).

8. Khudhur, J., Akroot, A., and Al-samari, A., "Experimental Investigation of Direct Solar Photovoltaics that Drives Absorption Refrigeration System", 1 (1): 116–135 (2023).

9. Jayathunga, D., Weliwita, J. A., Karunathilake, H., and Witharana, S., "Economic Feasibility of Thermal Energy Storage-Integrated Concentrating Solar Power Plants", ***Solar***, 3 (1): 132–160 (2023).

10. Kabeyi, M. J. B. and Olanrewaju, O. A., "Sustainable Energy Transition for Renewable and Low Carbon Grid Electricity Generation and Supply", ***Frontiers In Energy Research***, 9 (March): 1–45 (2022).

11. Tian, Y. and Zhao, C. Y., "A review of solar collectors and thermal energy storage in solar thermal applications", ***Applied Energy***, 104: 538–553 (2013).

12. Assaf, Y. H., Akroot, A., Abdul Wahhab, H. A., Talal, W., Bdaiwi, M., and Nawaf, M. Y., "Impact of Nano Additives in Heat Exchangers with Twisted Tapes and Rings to Increase Efficiency: A Review", ***Sustainability (Switzerland)***, 15 (10): (2023).

13. Alva, G., Lin, Y., and Fang, G., "An overview of thermal energy storage systems", ***Energy***, 144: 341–378 (2018).

14. Sarbu, I. and Sebarchievici, C., "A comprehensive review of thermal energy storage", ***Sustainability (Switzerland)***, 10 (1): (2018).

15. Dawood, T. A., Raphael, R., Barwari, I., and Akroot, A., "Solar Energy and Factors Affecting the Efficiency and Performance of Panels in Erbil / Kurdistan", 41 (2): 304–312 (2023).

16. Chidambaram, L. A., Ramana, A. S., Kamaraj, G., and Velraj, R., "Review of solar cooling methods and thermal storage options", ***Renewable And Sustainable Energy Reviews***, 15 (6): 3220–3228 (2011).

17. Kalaiarasi, G., Velraj, R., Vanjeswaran, M. N., and Ganesh Pandian, N., "Experimental analysis and comparison of flat plate solar air heater with and without integrated sensible heat storage", ***Renewable Energy***, 150: 255–265 (2020).

18. Wu, S., Zhou, C., Doroodchi, E., Nellore, R., and Moghtaderi, B., "A review on high-temperature thermochemical energy storage based on metal oxides redox cycle", ***Energy Conversion And Management***, 168 (March): 421–453 (2018).

19. Hamzah, A. H., Akroot, A., and Jaber, J. A., "Analytical Investigation of Biodiesel Mixed Levels and Operation Factors' Effects on Engine Performance by RCM", ***International Journal Of Design And Nature And Ecodynamics***, 17 (6): 863–873 (2022).

20. Wan, Z., Wei, J., Qaisrani, M. A., Fang, J., and Tu, N., "Evaluation on thermal and mechanical performance of the hot tank in the two-tank molten salt heat storage system", ***Applied Thermal Engineering***, 167 (December 2019): 114775 (2020).

21. Suresh, C. and Saini, R. P., .

22. Kalaiarasi, G., Velraj, R., Vanjeswaran, M. N., and Ganesh Pandian, N., "Experimental analysis and comparison of flat plate solar air heater with and without integrated sensible heat storage", ***Renewable Energy***, 150: 255–265 (2020).

23. Knobloch, K., Ulrich, T., Bahl, C., and Engelbrecht, K., "Degradation of a rock bed thermal energy storage system", ***Applied Thermal Engineering***, 214 (March): 118823 (2022).

24. Muhammad, Y., Saini, P., Knobloch, K., Lund, H., and Engelbrecht, K., "Rock bed thermal energy storage coupled with solar thermal collectors in an industrial application : Simulation , experimental and parametric analysis", ***Journal Of Energy Storage***, 67 (March): 107349 (2023).

25. Knobloch, K., Ulrich, T., Bahl, C., and Engelbrecht, K., "Degradation of a rock bed thermal energy storage system", ***Applied Thermal Engineering***, 214 (March): 118823 (2022).

26. Muhammad, Y., Saini, P., Knobloch, K., Lund, H., and Engelbrecht, K., "Rock bed thermal energy storage coupled with solar thermal collectors in an industrial application : Simulation , experimental and parametric analysis", ***Journal Of Energy Storage***, 67 (March): 107349 (2023).

27. Soprani, S., Marongiu, F., Christensen, L., Alm, O., Dinesen, K., Ulrich, T., and Engelbrecht, K., "Design and testing of a horizontal rock bed for high temperature thermal energy storage", ***Applied Energy***, 251 (April): 113345 (2019).

28. Marongiu, F., Soprani, S., and Engelbrecht, K., "Modeling of high temperature thermal energy storage in rock beds – Experimental comparison and parametric study", ***Applied Thermal Engineering***, 163 (February): 114355 (2019).

29. Nahhas, T., Py, X., and Sadiki, N., "Experimental investigation of basalt rocks as storage material for high- temperature concentrated solar power plants", ***Renewable And Sustainable Energy Reviews***, 110 (April): 226–235 (2019).

30. Desai, N. B., Mondejar, M. E., and Haglind, F., "Techno-economic analysis of two-tank and packed-bed rock thermal energy storages for foil-based concentrating solar collector driven cogeneration plants", ***Renewable Energy***, 186: 814–830 (2022).

31. Zanganeh, G., Pedretti, A., Zavattoni, S., Barbato, M., and Steinfeld, A., "Packed-bed thermal storage for concentrated solar power - Pilot-scale demonstration and industrial-scale design", ***Solar Energy***, 86 (10): 3084–3098 (2012).

32. Heller, L. and Gauché, P., "Modeling of the rock bed thermal energy storage system of a combined cycle solar thermal power plant in South Africa", ***Solar Energy***, 93: 345–356 (2013).

33. Pitot de la Beaujardiere, J. F. P., von Backström, T. W., and Reuter, H. C. R., "Applicability of the local thermal equilibrium assumption in the performance modelling of CSP plant rock bed thermal energy storage systems", ***Journal Of Energy Storage***, 15: 39–56 (2018).

34. Kocak, B. and Paksoy, H., "Performance of laboratory scale packed-bed thermal energy storage using new demolition waste based sensible heat materials for industrial solar applications", ***Solar Energy***, 211 (May): 1335–1346 (2020).

35. Abdulla, A. and Reddy, K. S., "Effect of operating parameters on thermal performance of molten salt packed-bed thermocline thermal energy storage system for concentrating solar power plants", ***International Journal Of Thermal***

Sciences, 121: 30–44 (2017).

36. Ozturk, M., Dincer, I., and Javani, N., "Thermodynamic modeling of a solar energy based combined cycle with rock bed heat storage system", ***Solar Energy***, 200 (May 2018): 51–60 (2020).

37. Sharma, A., Pandey, P. K., and Didwania, M., "Techno-economic optimization of packed-bed thermal energy storage system combined with CSP plant using DOE: design of experiment technique and Taguchi method", ***International Journal Of Energy And Environmental Engineering***, (0123456789): (2022).

38. Ortega-Fernández, I., Uriz, I., Ortuondo, A., Hernández, A. B., Faik, A., Loroño, I., and Rodríguez-Aseguinolaza, J., "Operation strategies guideline for packed bed thermal energy storage systems", ***International Journal Of Energy Research***, 43 (12): 6211–6221 (2019).

39. Abdulla, A. and Reddy, K. S., "Comparative study of single and multi-layered packed-bed thermal energy storage systems for CSP plants", ***Applied Solar Energy (English Translation Of Geliotekhnika)***, 53 (3): 276–286 (2017).

40. Saha, S. K. and Das, R. B., "Exergetic and performance analyses of two-layered packed bed latent heat thermal energy storage system", ***International Journal Of Energy Research***, 44 (3): 2208–2225 (2020).

41. Amiri, L., Ermagan, H., Kurnia, J. C., Hassani, F., and Sasmito, A. P., "Progress on rock thermal energy storage (RTES): A state of the art review", ***Energy Science And Engineering***, (April): (2023).

42. Rahbari, H. R., Arabkoohsar, A., and Alrobaian, A. A., "Thermodynamic, economic, and environmental analysis of a novel hybrid energy storage system: Psuedo-dynamic modeling approach", ***International Journal Of Energy Research***, 45 (14): 20016–20036 (2021).

43. Zhang, H., Liang, W., Liu, J., and Wang, J., "Modeling and Energy Efficiency Analysis of Thermal Power Plant with High Temperature Thermal Energy Storage (HTTES)", ***Journal Of Thermal Science***, 29 (4): 1025–1035 (2020).

44. Codd, D. S., Gil, A., Manzoor, M. T., and Tetreault-Friend, M., "Concentrating Solar Power (CSP)—Thermal Energy Storage (TES) Advanced Concept Development and Demonstrations", ***Current Sustainable/Renewable Energy Reports***, 7 (2): 17–27 (2020).

45. Guo, H., Xu, Y., Guo, C., Chen, H., Wang, Y., Yang, Z., Huang, Y., and Dou, B., "Thermodynamic Analysis of Packed Bed Thermal Energy Storage System", ***Journal Of Thermal Science***, 29 (2): 445–456 (2020).

46. Bhardwaj, V., Kaushik, S. C., and Garg, H. P., "Sensible thermal storage in rock beds for space conditioning: A state of the art study", ***International Journal Of Ambient Energy***, 20 (4): 211–219 (1999).

47. Kunwer, R. and Pandey, S., "Analysis and optimisation of packed bed thermocline

energy storage tank for CSP power plant", ***International Journal Of Ambient Energy***, 43 (1): 6081–6088 (2022).

48. Eddemani, A., Bammou, L., Tiskatine, R., Aharoune, A., Bouirden, L., and Ihlal, A., "Evaluation of the thermal performance of the air-rock bed solar energy storage system", ***International Journal Of Ambient Energy***, 42 (15): 1699–1707 (2021).

49. Yunus A Çengel, "Thermodynamics: An Engineering Approach", Angewandte Chemie International Edition, 6(11), 951–952., 2013–2015 (2003).

50. MORAN, M. J. and SHAPIRO, HOWARD N.BOETTNER, D. D. M. B. B., "Fundamentals of Engineering Thermodynamics", WILEY, 14–61 (2020).

51. Aghaziarati, Z. and Aghdam, A. H., "Thermoeconomic analysis of a novel combined cooling, heating and power system based on solar organic Rankine cycle and cascade refrigeration cycle", ***Renewable Energy***, 164: 1267–1283 (2021).

52. Tozlu, A., Kayabasi, E., and Ozcan, H., "Thermoeconomic analysis of a low-temperature waste-energy assisted power and hydrogen plant at off-NG grid region", ***Sustainable Energy Technologies And Assessments***, 52 (PA): 102104 (2022).

53. Ozturk, M., Dincer, I., and Javani, N., "Thermodynamic modeling of a solar energy based combined cycle with rock bed heat storage system", ***Solar Energy***, 200 (March 2019): 51–60 (2020).

54. Talal, W. . and Akroot, A., "Exergoeconomic Analysis of an Integrated Solar Combined Cycle in the Al-Qayara Power Plant in Iraq", ***Processes***, 11, 656.: (2023).

55. Demir, M. E. and Dincer, I., "Gas", ***International Journal Of Energy Research***, (2017).

56. Barakat, S., Ramzy, A., Hamed, A. M., and El Emam, S. H., "Enhancement of gas turbine power output using earth to air heat exchanger (EAHE) cooling system", ***Energy Conversion And Management***, 111: 137–146 (2016).

57. Abudu, K., Igie, U., Roumeliotis, I., and Hamilton, R., "Impact of gas turbine flexibility improvements on combined cycle gas turbine performance", ***Applied Thermal Engineering***, 189: 116703 (2021).

58. Akroot, A. and Nadeesh, A., "Performance Analysis of Hybrid Solid Oxide Fuel Cell-Gas Turbine Power System", (2021).

59. Akroot, A. and Namli, L., "Performance assessment of an electrolyte-supported and anode-supported planar solid oxide fuel cells hybrid system", ***J Ther Eng***, 7 (7): 1921–1935 (2021).

60. Akroot, A., "Effect of Operating Temperatures on the Performance of a SOFCGT

Hybrid System", ***International Journal Of Trend In Scientific Research And Development***, Volume-3 (Issue-3): 1512–1515 (2019).

61. Akroot, A., Namli, L., and Ozcan, H., "Compared Thermal Modeling of Anode- and Electrolyte-Supported SOFC-Gas Turbine Hybrid Systems", ***Journal Of Electrochemical Energy Conversion And Storage***, (2021).

62. Cao, Y., Zoghi, M., Habibi, H., and Raise, A., "Waste heat recovery of a combined solid oxide fuel cell - gas turbine system for multi-generation purposes", ***Applied Thermal Engineering***, 198: 117463 (2021).

63. Calise, F., Cappiello, F. L., Dentice d'Accadia, M., and Vicidomini, M., "Energy and economic analysis of a small hybrid solar-geothermal trigeneration system: A dynamic approach", ***Energy***, 208: 118295 (2020).

64. Nami, H., Mahmoudi, S. M. S., and Nemati, A., "Exergy, economic and environmental impact assessment and optimization of a novel cogeneration system including a gas turbine, a supercritical CO2 and an organic Rankine cycle (GT-HRSG/SCO2)", ***Applied Thermal Engineering***, 110: 1315–1330 (2017).

65. A Bejan, G Tsatsaronis, M. M., "Thermal Design and Optimization", Energy, 433–434 (1996).

66. Elmorsy, L., Morosuk, T., and Tsatsaronis, G., "Exergy-based analysis and optimization of an integrated solar combined-cycle power plant", ***Entropy***, 22 (6): 1–20 (2020).

67. Ozcan, H. and Kayabasi, E., "Thermodynamic and economic analysis of a synthetic fuel production plant via CO2 hydrogenation using waste heat from an iron-steel facility", ***Energy Conversion And Management***, 236 (February): 114074 (2021).

68. Mohammadkhani, F., Shokati, N., Mahmoudi, S. M. S., Yari, M., and Rosen, M. A., "Exergoeconomic assessment and parametric study of a Gas Turbine-Modular Helium Reactor combined with two Organic Rankine Cycles", ***Energy***, 65: 533–543 (2014).

69. Nourpour, M. and Khoshgoftar Manesh, M. H., "Evaluation of novel integrated combined cycle based on gas turbine-SOFC-geothermal-steam and organic Rankine cycles for gas turbo compressor station", ***Energy Conversion And Management***, 252 (January): 115050 (2022).

70. Kareem, A. F., Akroot, A., Wahhab, H. A. A., Talal, W., Ghazal, R. M., and Alfaris, A., "Exergo – Economic and Parametric Analysis of Waste Heat Recovery from Taji Gas Turbines Power Plant Using Rankine Cycle and Organic Rankine Cycle", (2023).

71. Lazzaretto, A. and Tsatsaronis, G., "SPECO: A systematic and general methodology for calculating efficiencies and costs in thermal systems", ***Energy***, 31 (8–9): 1257–1289 (2006).

72. Elsafi, A. M., "Exergy and exergoeconomic analysis of sustainable direct steam generation solar power plants", ***Energy Conversion And Management***, 103: 338–347 (2015).

73. Cavalcanti, E. J. C., .

74. Sanaye, S. and Yazdani, M., "Energy, exergy, economic and environmental analysis of a running integrated anaerobic digester-combined heat and power system in a municipal wastewater treatment plant", ***Energy Reports***, 8: 9724–9741 (2022).

75. Behzadi, A., Gholamian, E., Houshfar, E., and Habibollahzade, A., "Multi-objective optimization and exergoeconomic analysis of waste heat recovery from Tehran's waste-to-energy plant integrated with an ORC unit", ***Energy***, 160: 1055–1068 (2018).

76. Wang, S., Liu, C., Li, J., Sun, Z., Chen, X., and Wang, X., "Exergoeconomic analysis of a novel trigeneration system containing supercritical CO2 Brayton cycle, organic Rankine cycle and absorption refrigeration cycle for gas turbine waste heat recovery", ***Energy Conversion And Management***, 221 (May): 113064 (2020).

RESUME

Aya Ahmed FARAJ, in the Al Din Shirqat district, and attended the primary and high school there, after which she embarked on a Bachelor degree course at the University of Tikrit College of Engineering, Department of Mechanical Engineering, in 2013. In 2020, studies continued at the Karabük University Mechanical Engineering faculty to complete Master of Science degree studies.